nature neuroscience

SUPPLEMENTARY INFORMATION

https://doi.org/10.1038/s41593-018-0329-4

In the format provided by the authors and unedited.

Neutrophil adhesion in brain capillaries reduces cortical blood flow and impairs memory function in Alzheimer's disease mouse models

Jean C. Cruz Hernández[1,7], Oliver Bracko[1,7], Calvin J. Kersbergen[1], Victorine Muse[1], Mohammad Haft-Javaherian[1], Maxime Berg[2], Laibaik Park[3], Lindsay K. Vinarcsik[1], Iryna Ivasyk[1], Daniel A. Rivera[1], Yiming Kang[1], Marta Cortes-Canteli[4,5], Myriam Peyrounette[2], Vincent Doyeux[2], Amy Smith[2], Joan Zhou[1], Gabriel Otte[1], Jeffrey D. Beverly[1], Elizabeth Davenport[1], Yohan Davit[2], Charles P. Lin[6], Sidney Strickland[4], Costantino Iadecola[3], Sylvie Lorthois[1,2], Nozomi Nishimura[1,8*] and Chris B. Schaffer[1,8*]

[1]Nancy E. and Peter C. Meinig School of Biomedical Engineering, Cornell University, Ithaca, NY, USA. [2]Institut de Mécanique des Fluides de Toulouse, Université de Toulouse, CNRS, INPT, UPS, Toulouse, France. [3]Feil Family Brain and Mind Research Institute, Weill Cornell Medicine, New York, NY, USA. [4]Patricia and John Rosenwald Laboratory for Neurobiology and Genetics, The Rockefeller University, New York, NY, USA. [5]Centro Nacional de Investigaciones Cardiovasculares Carlos III, Madrid, Spain. [6]Wellman Center for Photomedicine and Center for Systems Biology, Massachusetts General Hospital, Harvard Medical School, Boston, MA, USA. [7]These authors contributed equally: Jean C. Cruz Hernández, Oliver Bracko. [8]These authors jointly supervised this work: Nozomi Nishimura, Chris B. Schaffer. *e-mail: nn62@cornell.edu; cs385@cornell.edu

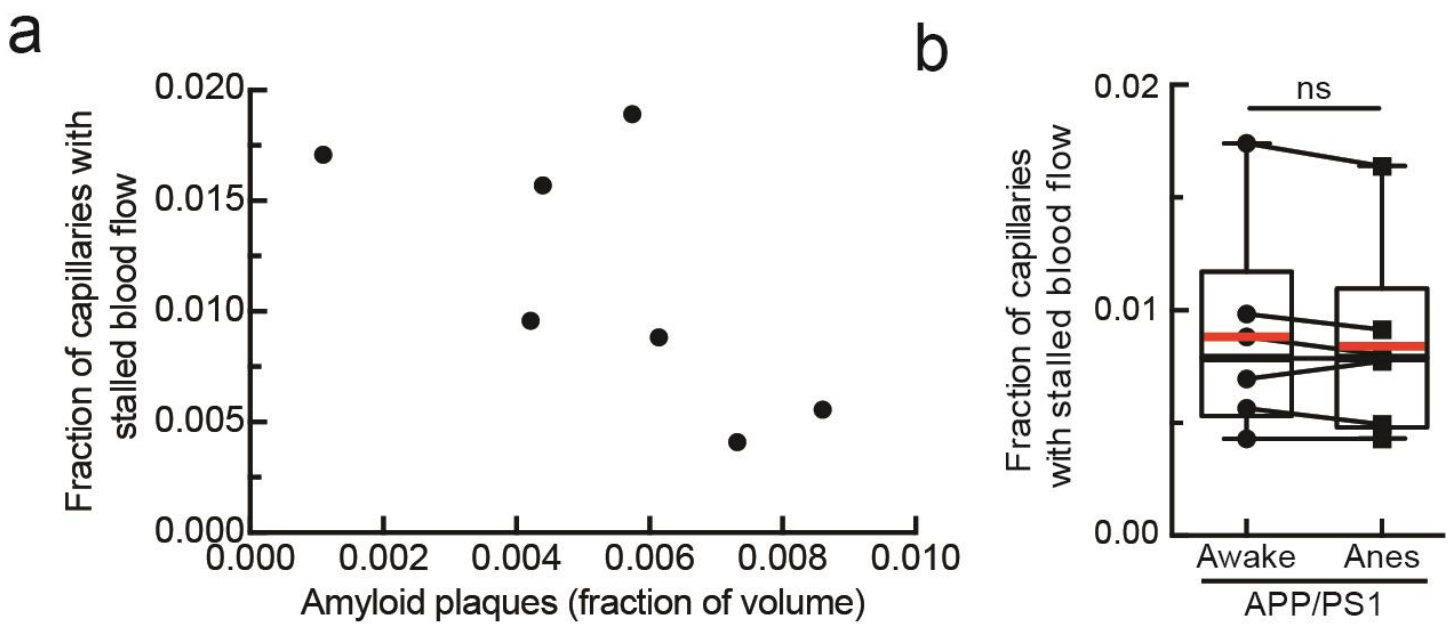

Supplementary Figure 1

Capillary stalling in APP/PS1 mice was not influenced by anesthesia or modulated by amyloid plaque density.

(a) The fraction of capillaries with stalled blood flow did not increase with increasing cortical amyloid plaque density in APP/PS1 mice. Fraction of capillaries with stalled blood flow as a function of the cortical volume fraction that was labeled by methoxy-X04. Mice ranged from 50 to 64 weeks of age with 4 females and 3 males. (b) Plot of the fraction of capillaries with stalled blood flow in mice imaged while anesthetized and awake. Lines connecting data points indicate data from the same animal. Animals were first trained to remain calm while head fixed and standing on a spherical treadmill. On the day of imaging, animals were briefly anesthetized to enable retro-orbital injection of Texas-Red dextran, and were then allowed to wake up. We imaged these animals first while awake and then while anesthetized under 1.5% isoflurane, with both imaging sessions occurring on the same day (10-month old APP/PS1 mice; n=6 (5 female, 1 male); p=0.31 no significant difference by two-tailed, matched pairs signed rank Wilcoxon test; Boxplots are defined as: whiskers extend 1.5 times the difference between the value of the 75th and 25th percentile, median=black line and mean= red line).

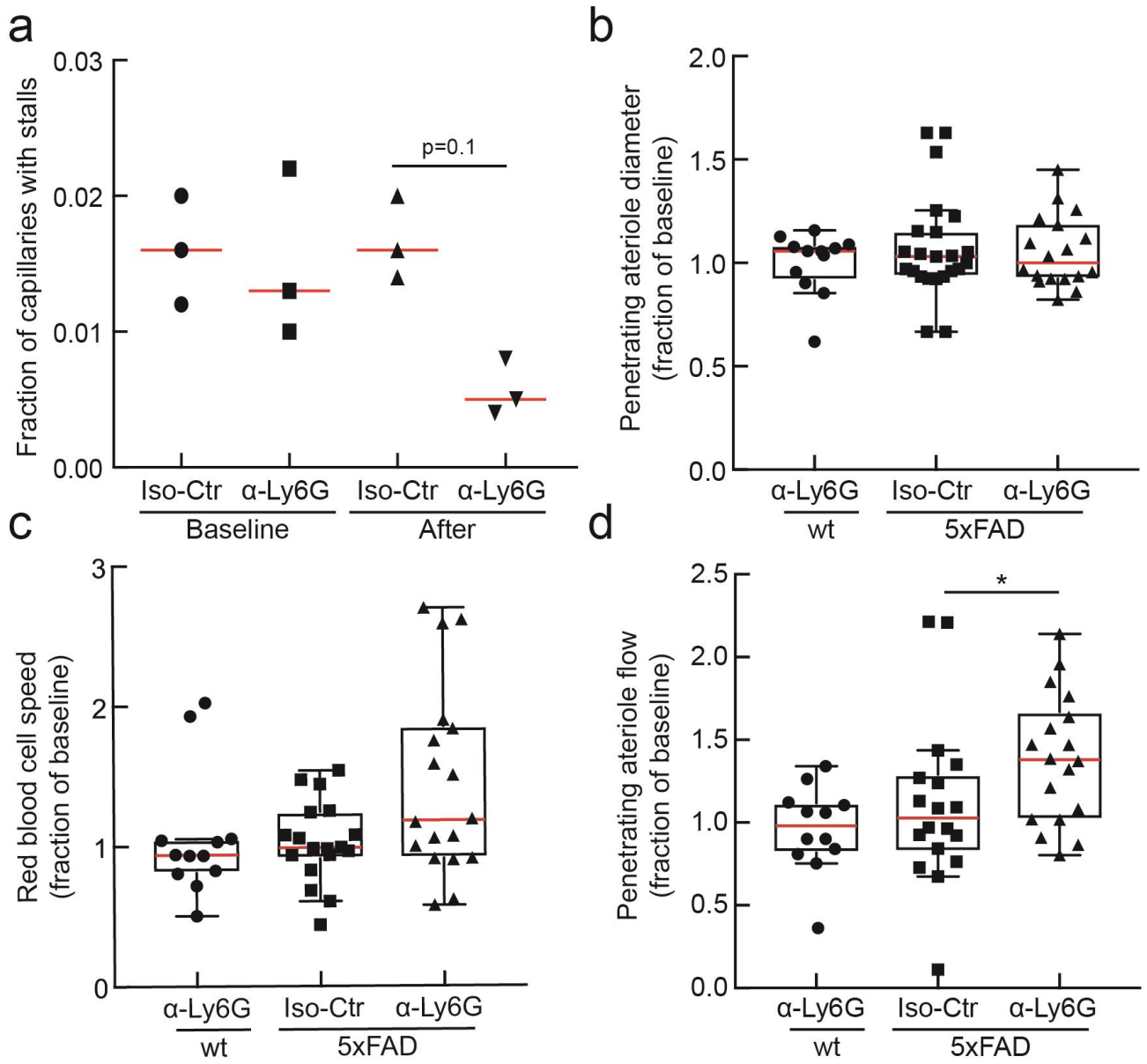

Supplementary Figure 2

α-Ly6G administration reduced the number of cortical capillary stalls and increased penetrating arteriole blood flow in 5xFAD mice.

(a) Fraction of capillaries with stalled blood flow in 5-7 month old 5xFAD mice at baseline and at about one hour after injection of α-Ly6G or isotype control antibodies (5xFAD Iso-Ctr: n=3 (2 female, 1 male); and 5xFAD α-Ly6G: n=3 (1 female, 2 male); two-tailed Mann-Whitney p=0.10; mean= red line). (b) Vessel diameter, (c) RBC flow speed, and (d) RBC volumetric blood flow from cortical penetrating arterioles after α-Ly6G or isotype control antibody administration, shown as a fraction of the baseline value, in 5xFAD or wild-type mice (wild-type α-Ly6G: n=3 (1 female, 2 male), 13 arterioles; 5xFAD Iso-Ctr: n=3 (2 female, 1 male), 18 arterioles; and 5xFAD α-Ly6G: n=3 (1 female, 2 male), 19 arterioles; one way Kruskal-Wallis ANOVA with post-hoc pair-wise comparisons using Dunn's multiple comparison test: penetrating arteriole flow (panel d) 5xFAD Iso-Ctrl vs. 5xFAD α-Ly6G p=0.023; no other significant differences). Boxplots are defined as: whiskers extend 1.5 times the difference between the value of the 75th and 25th percentile, median=black line and mean= red line).

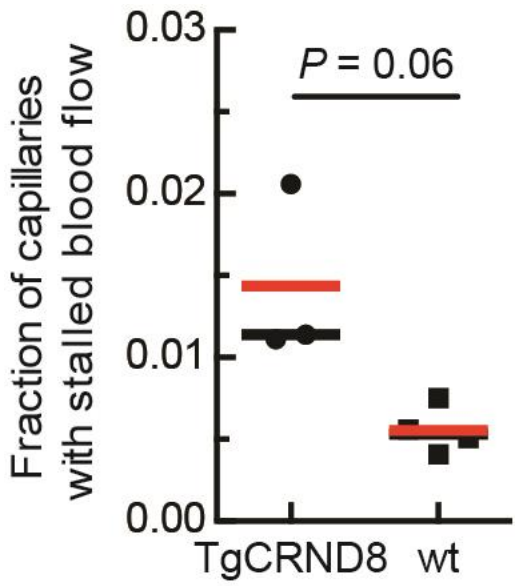

Supplementary Figure 3

2PEF imaging of cortical vasculature reveals a higher fraction of stalled capillaries in TgCRND8 mice as compared to WILD-TYPE mice.

Fraction of capillaries with stalled blood flow in TgCRND8 and age-matched wild type littermates (TgCRND8: n=3 (all female), 3,028 capillaries; wild type: n=4 (all female), 4,062 capillaries; p=0.06, Two-tailed Mann-Whitney; median=black line and mean= red line).

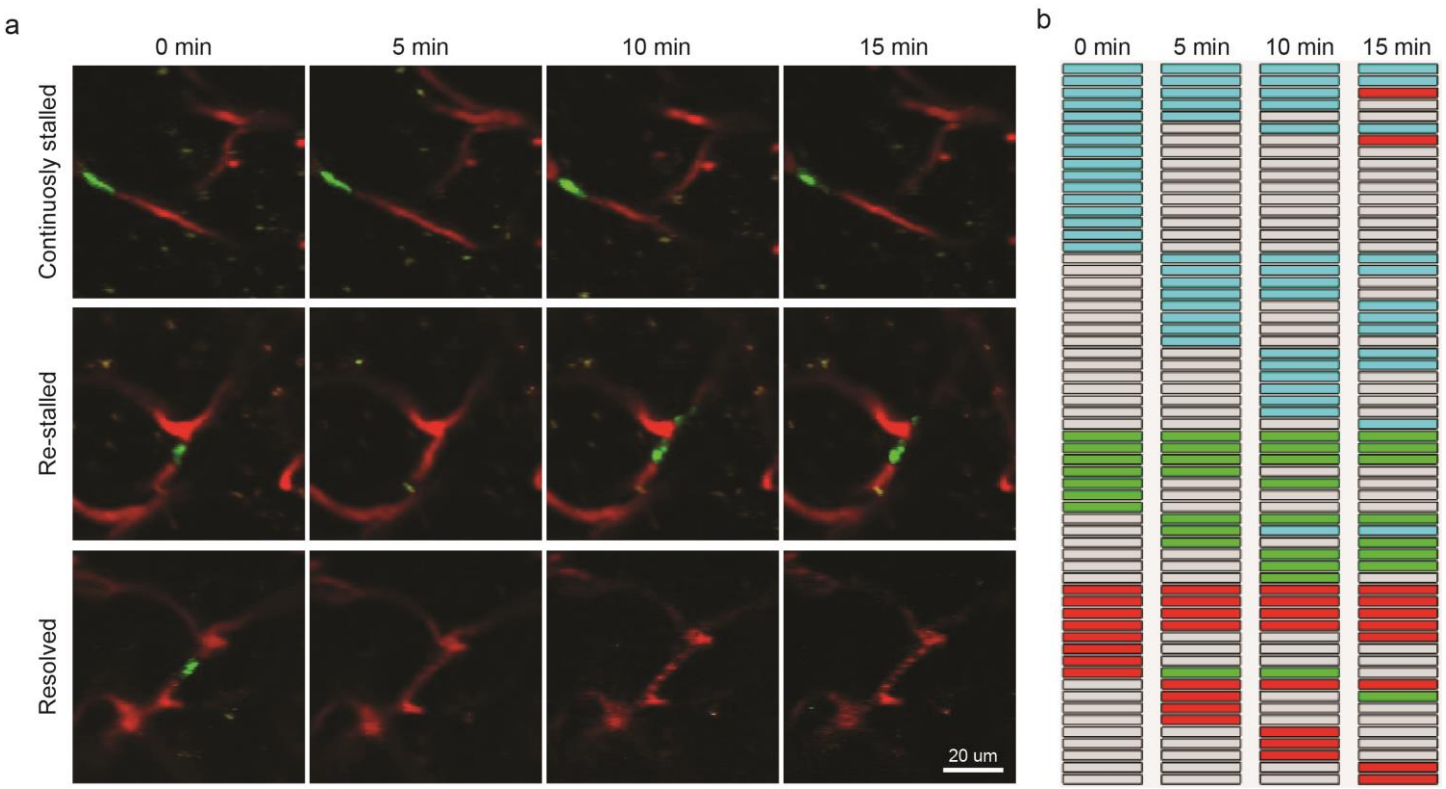

Supplementary Figure 4

Characterization of capillary stall dynamics in APP/PS1 mice.

(a) Repeated 2PEF imaging over 15 min of capillaries that were stalled at the baseline measurement and (top) remained stalled, (middle) began flowing and then re-stalled and (bottom) resolved and remained flowing. Blood plasma labeled with Texas-Red dextran (red) and leukocytes labeled with Rhodamine 6G (green). (b) Characterization of the fate of individual capillaries observed as being stalled across four image stacks taken at baseline and 5, 10, and 15 min later. Each row represents an individual capillary and the color of the box for each capillary at each time point indicates the status: flowing (grey), stalled with a leukocyte present (cyan), stalled with platelet aggregates present (green), and stalled with only RBCs (red). Note that unlike the results shown in Fig. 3b, we do not separate cases where RBCs are present along with a leukocyte or platelet aggregates (n =2 mice (all female), 61 capillaries).

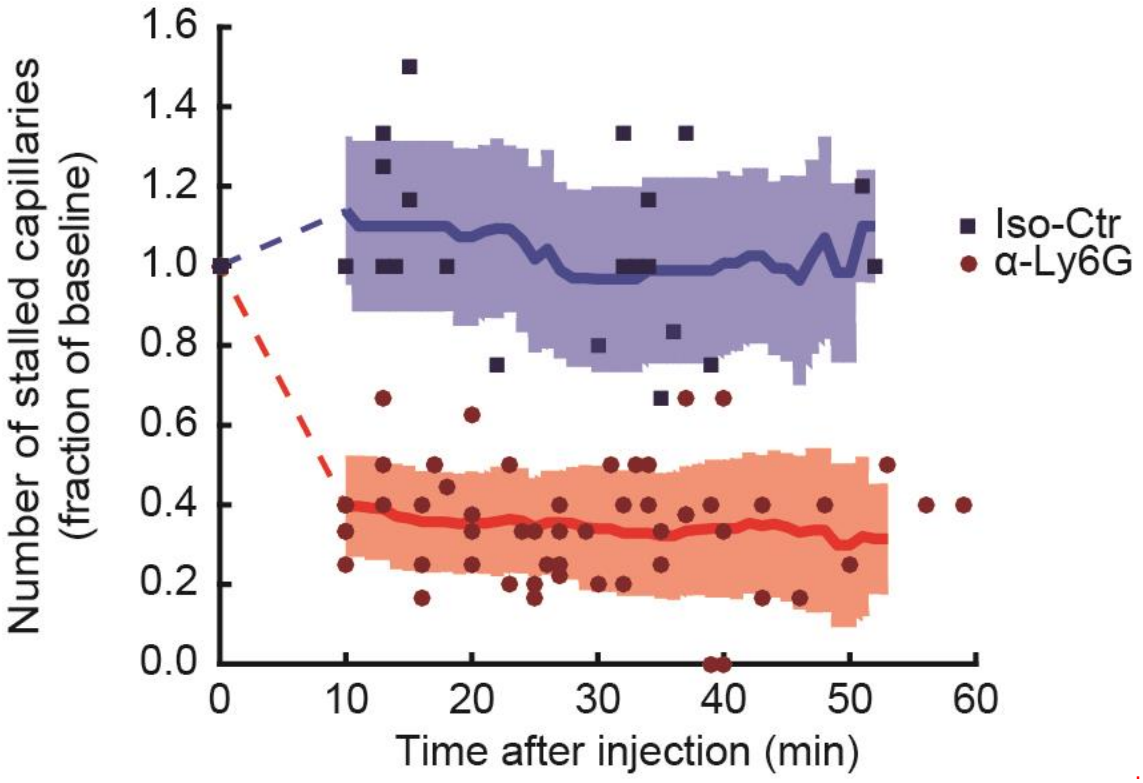

Supplementary Figure 5

Number of stalled capillaries in APP/PS1 mice dropped rapidly after α-Ly6G administration.

2PEF image stacks were taken repeatedly over an hour after α-Ly6G or isotype control antibody injection and the number of stalled capillaries determined at each time point (α-Ly6G: n=6 mice (5 female, 1 male); Iso-Ctr: n=4 mice (3 female, 1 male); each mouse imaged 2 to 6 times over the hour; lines represents sliding averages and shaded areas represent 95% confidence intervals).

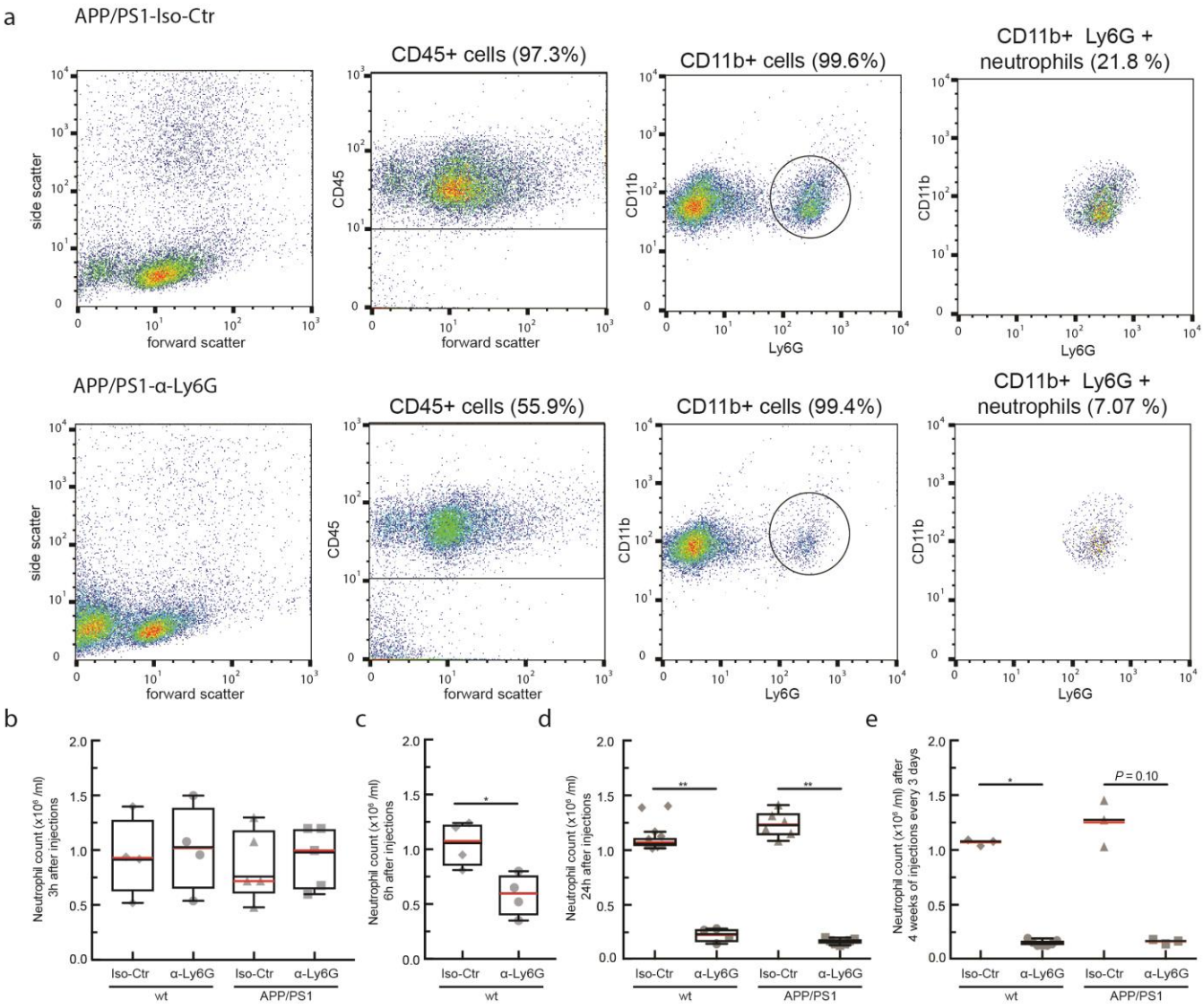

Supplementary Figure 6

Treatment with α-Ly6G leads to neutrophil depletion in both APP/PS1 and wild-type control mice, beginning more than 3 h after administration.

(a) Representative flow cytometry data for blood drawn from APP/PS1 mice 24 hours after treatment with isotype control antibodies (top row) and α-Ly6G (bottom row). Left column shows forward and side scattering from entire population of blood cells (after lysing and removing red blood cells). The second column shows the gate on CD45+ cells, indicating leukocytes. The third column shows expression of CD11b (high for monocytes and neutrophils) and Ly6G (high for neutrophils) for the CD45+ cells. Cells with high expression levels of both CD11b and Ly6G were considered to be neutrophils (right column). (b-d) Neutrophil counts for APP/PS1 and wild-type mice 3, 6, and 24 hr after a single treatment with α-Ly6G or isotype control antibodies, respectively. (3 hr data: wild-type Iso-Ctr: n=4 (3 female, 1 male); wild-type α-Ly6G: n=4 (2 female, 2 male); APP/PS1 Iso-Ctr: n=4 (2 female, 2 male); APP/PS1 α-Ly6G: n=5 (2 female, 3 male); two-tailed Mann-Whitney, no significant differences) (6 hr data: wild-type Iso-Ctr: n=4 (2 female, 3 male); wild-type α-Ly6G: n=4 (3 female, 1 male); two-tailed Mann-Whitney, p=0.029) (24 hr data: wild-type Iso-Ctr: n=9 (8 female, 1 male); wild-type α-Ly6G: n=4 (all female); APP/PS1 Iso-Ctr: n=6 (3 female, 3 male); APP/PS1 α-Ly6G: n=7 (2 female, 5 male); two-tailed Mann-Whitney: wild-type Iso-Ctr vs. wild-type α-Ly6G p=0.0028, APP/PS1 Iso-Ctr vs. APP/PS1 α-Ly6G p=0.0012) (e) Neutrophil counts for APP/PS1 and wild-type mice after one month of treatment with α-Ly6G or isotype control antibodies every three days (4 week data: wild-type Iso-Ctr: n=3 (2 female, 1 male); wild-type α-Ly6G: n=7 (6 female, 1 male); APP/PS1 Iso-Ctr: n=3 (1 female, 2 male); APP/PS1 α-Ly6G: n=3 (2 female, 1 male); two-tailed Mann-Whitney: wild-type Iso-Ctr vs. wild-type α-Ly6G p=0.017, APP/PS1 Iso-Ctr vs. APP/PS1 α-Ly6G p=0.10; median=black line and mean= red line). All boxplots are defined as: whiskers extend 1.5 times the difference between the value

of the 75th and 25th percentile, median=black line and mean= red line.

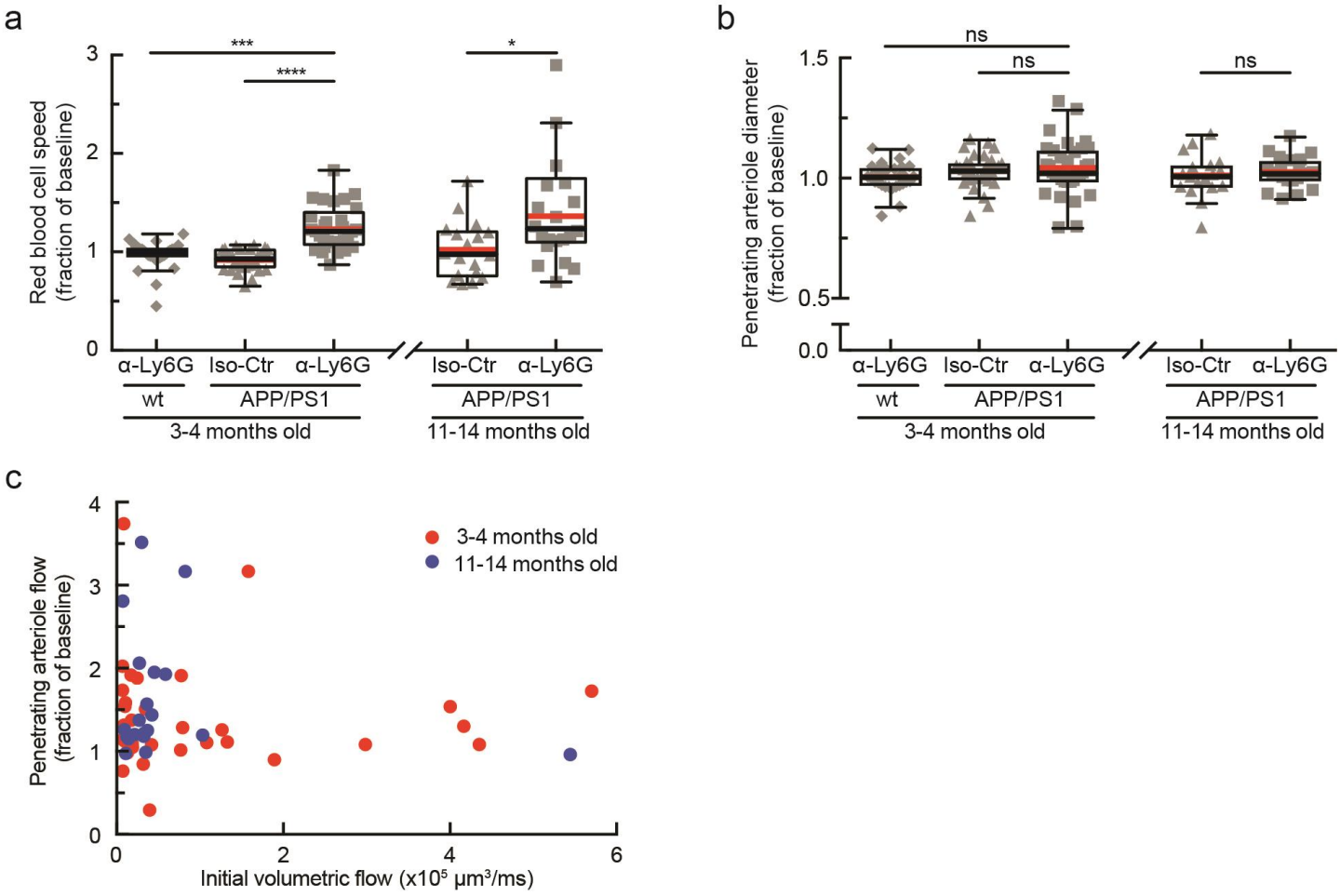

Supplementary Figure 7

Administration of antibodies against Ly6G increased the RBC flow speed but did not alter the diameter of cortical penetrating arterioles in APP/PS1 mice.

(a) RBC flow speed and (b) vessel diameter of penetrating arterioles after α-Ly6G or isotype control antibody administration in young (3-4 months) and old (11-14 months) APP/PS1 mice and wild-type control animals shown as a fraction of baseline (young APP/PS1 Iso-Ctr: n = 5 mice (1 female, 4 male), 32 arterioles; old APP/PS1 Iso-Ctr: n = 3 mice (1 female, 2 male), 18 arterioles; young wild-type α-Ly6G: n = 5 mice (3 female, 2 male), 30 arterioles; young APP/PS1 α-Ly6G: n = 5 (2 female, 3 male), 33 arterioles; old APP/PS1 α-Ly6G: n = 3 mice (all male), 22 arterioles; one-way Kruskal-Wallis ANOVA with post-hoc using Dunn's multiple comparison correction: for RBC speed data (panel a): young wild-type α-Ly6G vs. young APP/PS1 α-Ly6G p = 0.00014; young APP/PS1 Iso-Ctr vs. young APP/PS1 α-Ly6G p = 3.7×10^{-8}; old APP/PS1 Iso-Ctr vs. old APP/PS1 α-Ly6G p = 0.027; for vessel diameter data (panel b): no significant differences). All boxplots are defined as: whiskers extend 1.5 times the difference between the value of the 75th and 25th percentile, median=black line and mean= red line. (c) Penetrating arterioles with slower initial flow tended to increase flow speed more after α-Ly6G injection in APP/PS1 mice. Plot of penetrating arteriole flow after α-Ly6G antibody administration in young (3-4 months) and old (11-14 months) APP/PS1 mice shown as a fraction of baseline flow. Same data as shown in Fig. 3c.

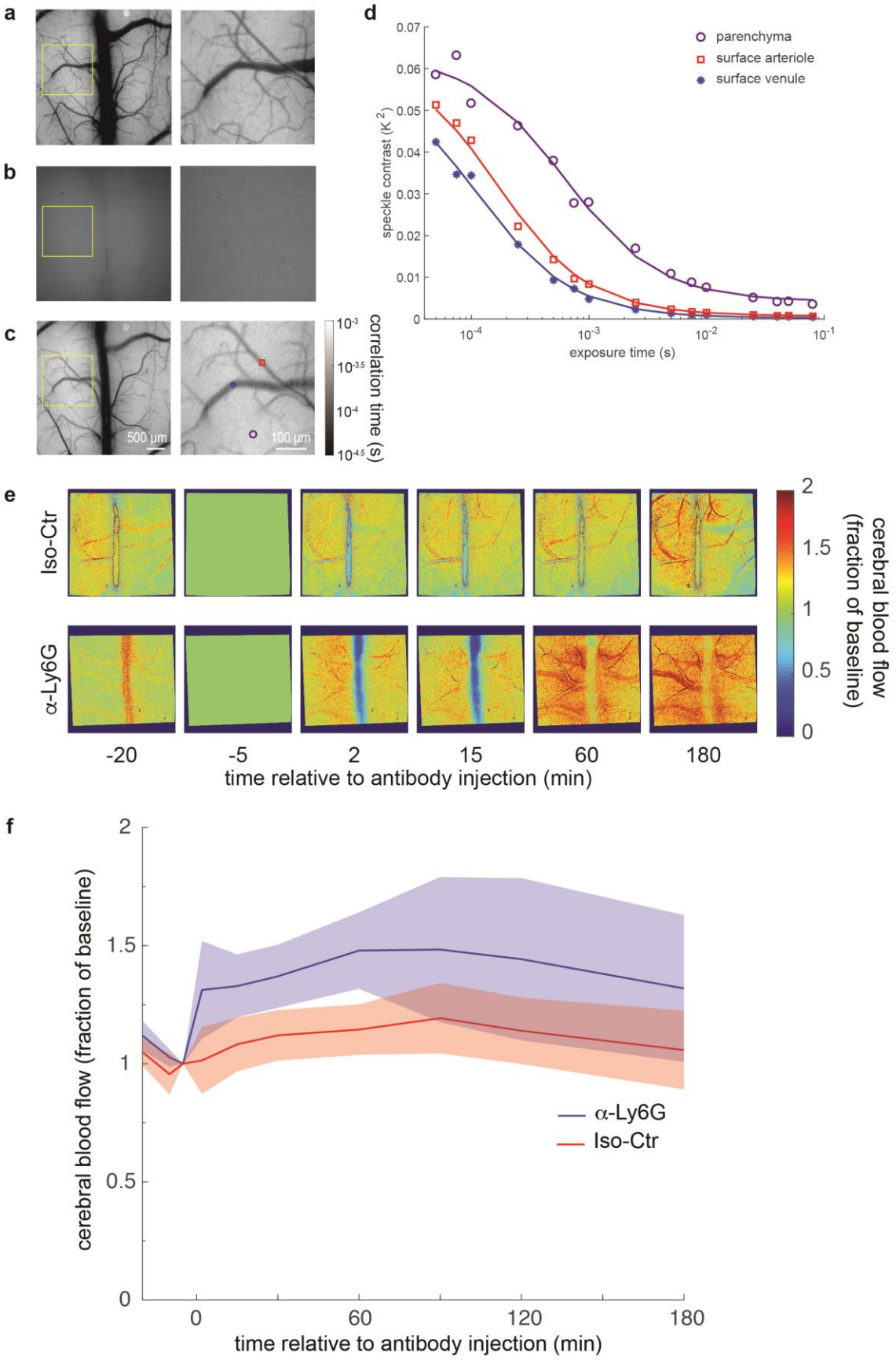
a
b
c
d
e
f
500 µm
100 µm
correlation time (s)
parenchyma
surface arteriole
surface venule
speckle contrast (K 2)
exposure time (s)
Iso-Ctr
α-Ly6G
-20
-5
2
15
60
180
time relative to antibody injection (min)
cerebral blood flow (fraction of baseline)
α-Ly6G
Iso-Ctr

Supplementary Figure 8

Multi-exposure laser speckle imaging revealed CBF increased in APP/PS1 mice within minutes of α-Ly6G administration.

(a) Green light reflectance image of parietal cortex of APP/PS1 mouse. Image to the right is a expanded view of the region outlined with a yellow box. (b) Raw laser speckle image of the same region as (a) with a 10 ms exposure time. (c) Correlation time image of the same region as (a). (d) Speckle contrast values as a function of image exposure time, showing fits for regions of interest located in a surface arteriole, surface venule, or parenchymal region. The corresponding symbols in the expanded view of (c) show the locations for each fit. (e) Images and (f) plot of cerebral blood flow as a function of time after antibody injection, expressed as a fraction of the value at 5 minutes before injection for APP/PS1 mice treated with isotype control antibodies or α-Ly6G. (APP/PS1 α-Ly6G: 5 mice (2 female, 3 male); APP/PS1 Iso-Ctrl: 5 mice (1 female, 4 male); age range 9-19 months; shaded regions represent the standard deviation).

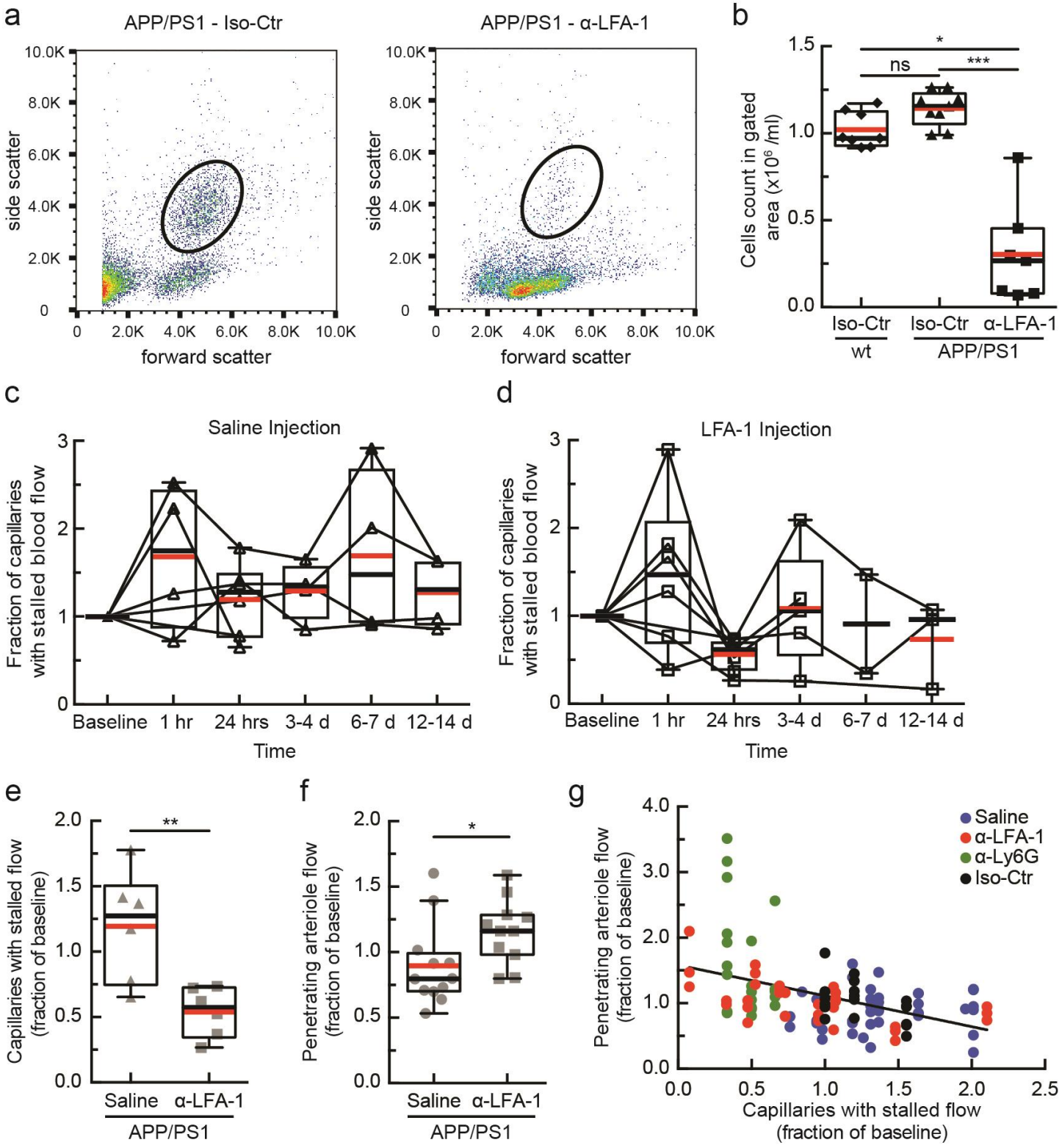

Supplementary Figure 9

Treating APP/PS1 mice with α-LFA-1 reduced the number of stalled capillaries and improved arterial blood flow after 24 h.

(a) Flow cytometry scatter plots for APP/PS1 mice 24 hours after injection of isotype control antibodies (left) or with antibodies against

Lymphocyte Functional Antigen 1 (α-LFA-1; M17/4 clone, BD Biosciences; 4 mg/kg, retro-orbital injection). Circles depict the gate used to identify leukocytes. (b) Leukocyte concentration in the blood 24 hours after treatment with α-LFA-1 or isotype control antibodies in APP/PS1 and wild-type mice. Leukocytes counts in the gating area were decreased by 84% after α-LFA-1 as compared to the isotype control in APP/PS1 mice (wild-type Iso-Ctr: n=8 (4 female, 4 male), APP/PS1 Iso-Ctr: n=9 (4 female, 5 male), APP/PS1 α-LFA-1: n=7 (4 female, 3 male); one-way Kruskal-Wallis ANOVA with post-hoc pair-wise comparisons using Dunn's multiple comparison test: wild-type Iso-Ctr vs. APP/PS1 α-LFA-1 p=0.046, APP/PS1 Iso-Ctr vs. α-LFA-1 p=0.00010). (c and d) Fraction of capillaries with stalled blood flow as a function of time after a single retro-orbital treatment with 0.9% saline (c) or α-LFA-1 antibodies (d) in APP/PS1 mice (saline: n=6 mice (2 female, 4 male); α-LFA-1: n=7 mice (3 female, 4 male), 4 mg/kg). We observed a transient increase in the number of capillaries with stalled blood flow at about 1 hr after treatment in both groups. There was a significant decrease in the fraction of stalled capillaries 24 hours after injection in the α-LFA-1 group. Images were collected over the same capillary bed on each imaging day, and the fraction of capillaries stalled was determined for each time point, with the analysis performed blinded to treatment day and treatment type. (e) Number of stalled capillaries, expressed as a fraction of the baseline number, 24 hrs after administration of α-LFA-1 or saline in APP/PS1 mice. α-LFA-1 reduced capillary stalls by 65% as compared to the saline control. (α-LFA-1 n = 6 mice, saline n = 6 mice; two-tailed Mann-Whitney test p=0.019). (f) Fraction of baseline arteriole flow in penetrating arterioles from APP/PS1 mice 24 hours after α-LFA-1 or saline treatment. Each point represents a single arteriole in one mouse. The blood flow was increased after α-LFA-1 treatment by 29% compared with saline controls (α-LFA1: n=4 mice, 11 arterioles; saline: n=4 mice, 12 arterioles; two-tailed Mann-Whitney test p=0.016). Boxplots are defined as: whiskers extend 1.5 times the difference between the value of the 75th and 25th percentile, median=black line and mean= red line. (g) Brain penetrating arteriole blood flow negatively correlates with the number of capillaries stalled in underlying capillary beds in APP/PS1 mice. To correlate the effect of capillary stalling on penetrating arteriole blood flow, we imaged the same capillaries and measured blood flow in the same penetrating arterioles in APP/PS1 mice multiple times before and after administration of saline, α-LFA-1, α-Ly6G, and isotype control antibodies. For saline and α-LFA-1 animals, there were measurements at multiple time points over two weeks (data in Supplementary Fig. 9). For α-Ly6G and isotype control animals there were measurements only at baseline and ~1 hr after administration (data in Fig. 3c and Supplementary Figs. 7). For each penetrating arteriole at each imaged time point, we plotted the volumetric flow, expressed as a fraction of the baseline volumetric flow, as a function of the number of capillaries stalled at that time point, expressed as a fraction of the baseline number of capillaries stalled (APP/PS1 α-LFA1: n=4 mice, 11 arterioles; APP/PS1 saline: n=4 mice, 12 arterioles; APP/PS1 α-Ly6G: n=3 mice, 22 arterioles; APP/PS1 Iso-Ctr: n=3 mice, 18 arterioles). These data confirm the sensitive dependence of penetrating arteriole blood flow on the fraction of capillaries with stalled flow across several different manipulations that led to either increases or decreases in the fraction of capillaries that are stalled. The linear regression is defined by: $Y = -0.47 X + 1.6$ ($R^2 = 0.2$, goodness of fit test; 95% confidence interval on slope: -0.65 – -0.29).

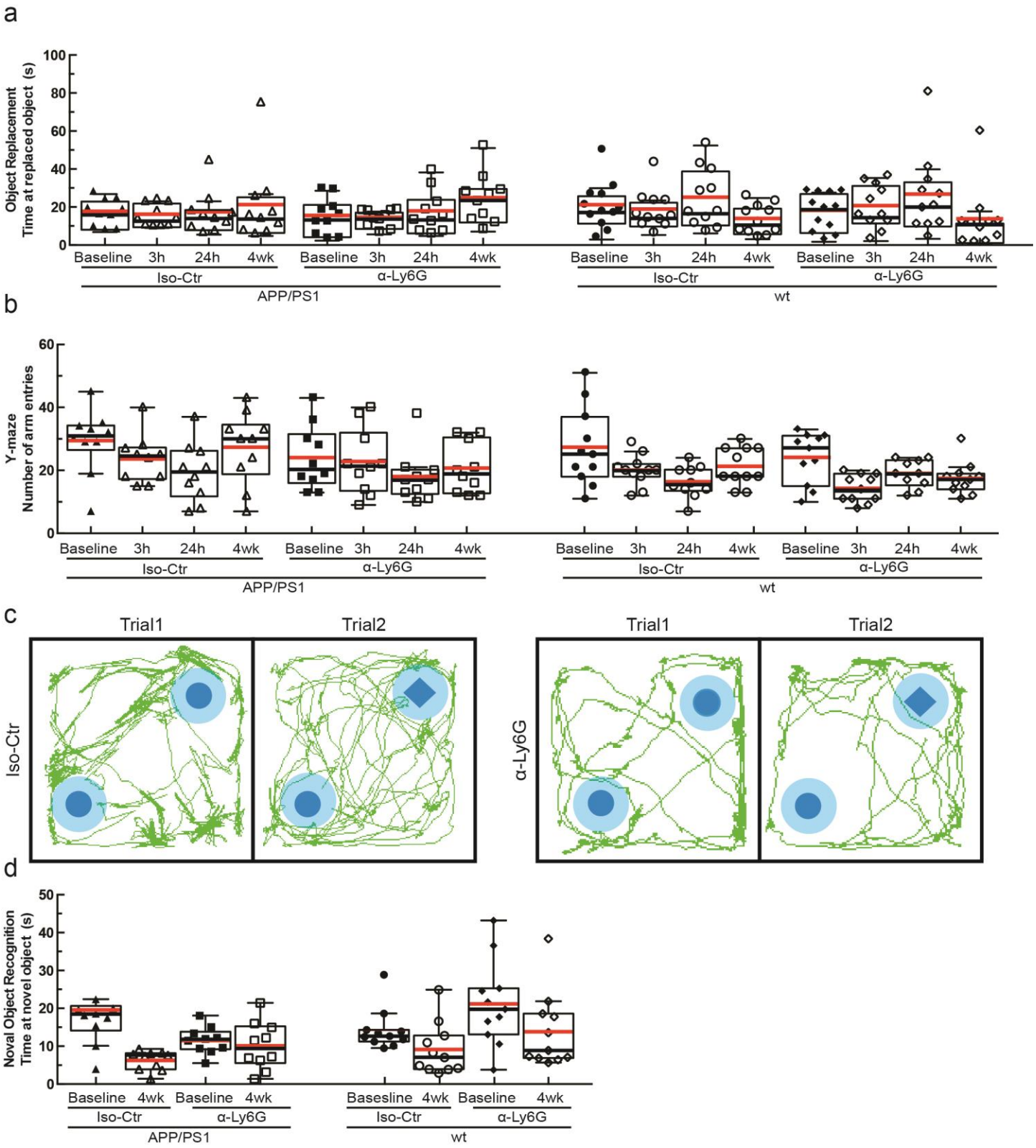

Supplementary Figure 10

Repeated behavioral testing did not significantly impair exploratory behavior.

(a) Time spent at the replaced object measured over 6 minutes for APP/PS1 and wild-type mice at baseline and at 3h and 24h after a single administration of α-Ly6G or isotype control antibodies, and after 4 weeks of treatment every three days (APP/PS1 Iso-Ctr: n=10 mice (5 female, 5 female), APP/PS1 α-Ly6G: n=10 mice (5 female, 5 male), wild-type α-Ly6G: n=11 mice (7 female, 4 male), wild-type Iso-Ctr: n=11 mice (8 female, 3 male); no significant differences among groups as determined by one-way Kruskal-Wallis ANOVA). (b) Number of arm entries in the Y-maze measured for 6 minutes for APP/PS1 and wild-type mice at baseline and at 3h and 24h after a single administration of α-Ly6G or isotype control antibodies, and after 4 weeks of treatment every three days (APP/PS1 Iso-Ctr: n=10 mice (5 female, 5 female), APP/PS1 α-Ly6G: n=10 mice (5 female, 5 male), wild-type α-Ly6G: n=11 mice (7 female, 4 male), wild-type Iso-Ctr: n=11 mice (8 female, 3 male); no significant differences among groups as determined by one-way Kruskal-Wallis ANOVA). (c) Representative map of animal location and time spent at the novel object in wild type controls and APP/PS1 animals treated with α-Ly6G or isotype control antibodies. Tracking of mouse nose location from video recording during training and trial phases of novel object recognition task taken 4 weeks after administration of α-Ly6G or isotype control antibodies every three days in APP/PS1 mice. (d) Time spent at the novel object (APP/PS1 Iso-Ctr: n=10 mice (5 female, 5 female), APP/PS1 α-Ly6G: n=10 mice (5 female, 5 male), wild-type α-Ly6G: n=11 mice (7 female, 4 male), wild-type Iso-Ctr: n=11 mice (8 female, 3 male); no significant differences among groups as determined by one-way Kruskal-Wallis ANOVA). Boxplots are defined as: whiskers extend 1.5 times the difference between the value of the 75th and 25th percentile, median=black line and mean= red line. All data in this figure represents the aggregation of two independently-conducted sets of behavioral experiments.

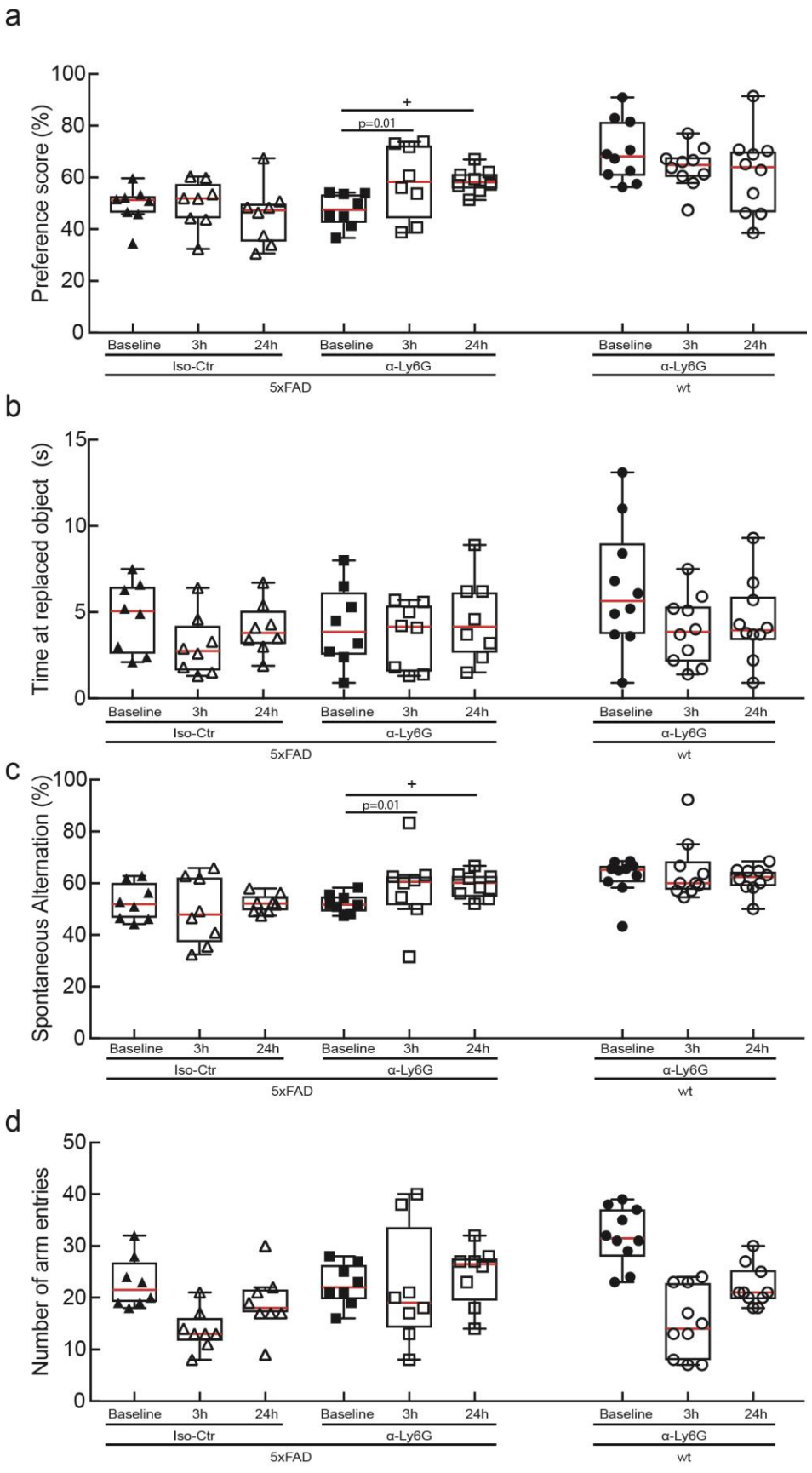
a
Preference score (%)
100
80
60
40
20
0
+
p=0.01
Baseline
3h
24h
Iso-Ctr
α-Ly6G
5xFAD
wt
b
Time at replaced object (s)
15
10
5
0
c
Spontaneous Alternation (%)
d
Number of arm entries
50
40
30
20
10

Supplementary Figure 11

Administration of α-Ly6G improves performance of 5xFAD mice on object replacement and Y-maze tests of spatial and working memory.

(a) Preference score in OR task at baseline and at 3 hr and 24 hr after a single administration of α-Ly6G or Iso-Ctr antibodies. (b) Time spent at the replaced object measured over 3 minutes for 5xFAD and wild-type mice at baseline and at 3h and 24h after a single administration of α-Ly6G or isotype control antibodies. (c) Spontaneous alternation in Y-Maze task at baseline and at 3 hr and 24 hr after a single administration of α-Ly6G or Iso-Ctr antibodies. (d) Number of arm entries in the Y-maze measured for 6 minutes for 5xFAD and wild-type mice at baseline and at 3h and 24h after a single administration of α-Ly6G or isotype control antibodies. (5xFAD α-Ly6G: n=8 mice (4 female, 4 male); 5xFAD Iso-Ctr: n=8 mice (3 female, 5 male); and wild-type α-Ly6G: n=10 mice (4 female, 6 male); Friedman one-way repeated measures non-parametric ANOVA to compare baseline and after treatment results within a group: Object replacement 5xFAD α-Ly6G (panel a) baseline vs. 3h p=0.091, baseline vs. 24h p=0.025; Y-maze 5xFAD α-Ly6G (panel c) baseline vs. 3h p=0.091, baseline vs 24h p=0.025. Note that the ranks of the data values in the object replacement and Y-maze were the same between these separate experiments, yielding the identical p-values.) Boxplots are defined as: whiskers extend 1.5 times the difference between the value of the 75th and 25th percentile, median=black line and mean= red line.

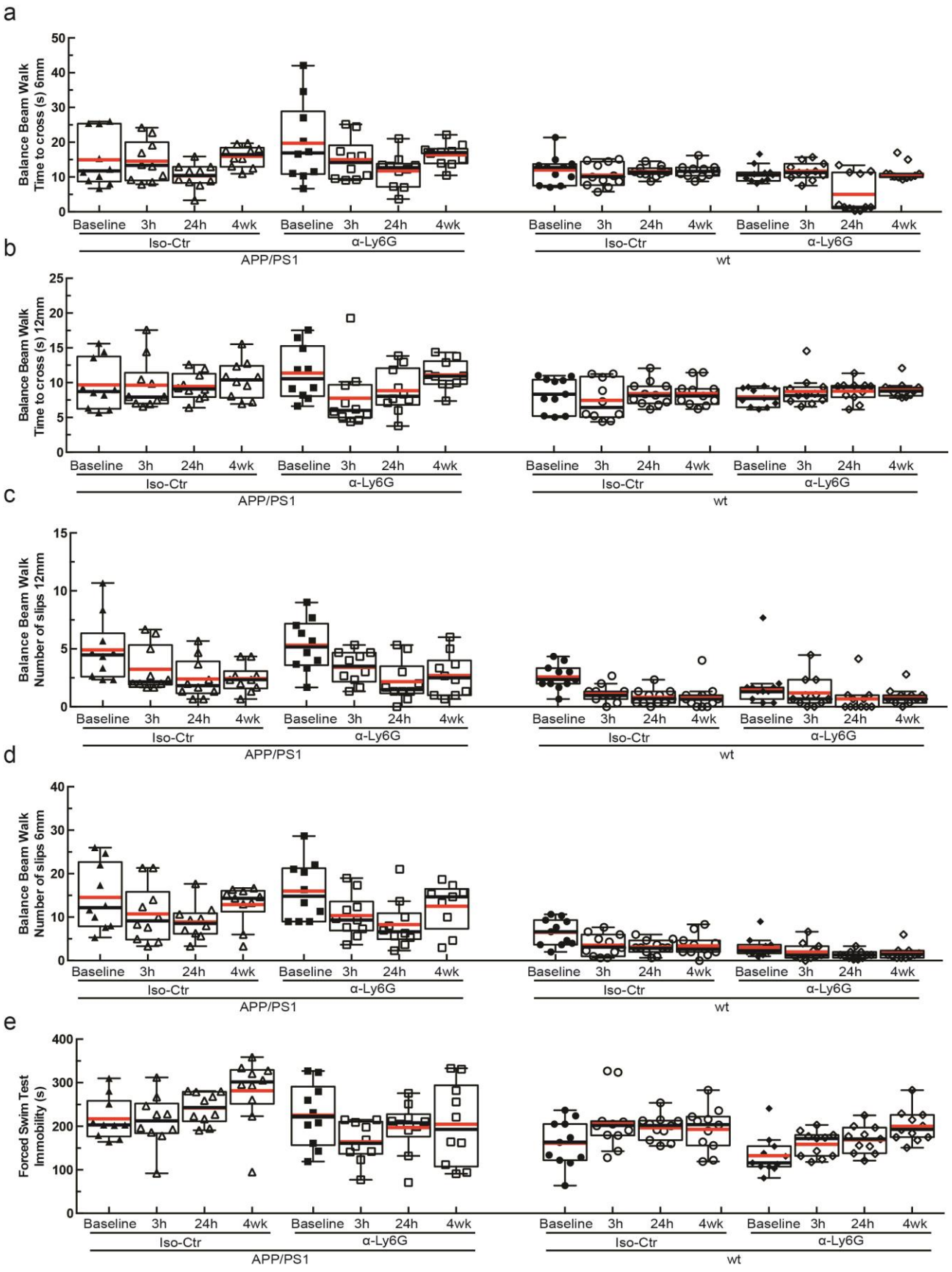
a
Balance Beam Walk
Time to cross (s) 6mm
b
Balance Beam Walk
Time to cross (s) 12mm
c
Balance Beam Walk
Number of slips 12mm
d
Balance Beam Walk
Number of slips 6mm
e
Forced Swim Test
Immobility (s)
Baseline
3h
24h
4wk
Iso-Ctr
α-Ly6G
APP/PS1
wt

Supplementary Figure 12

Balance beam walk (BBW) to measure motor coordination and forced swim test to measure depression-like behavior in wild-type controls and APP/PS1 animals treated with α-Ly6G or isotype control antibodies.

(a and b) BBW time to cross on a 6- and 12-mm diameter beam, respectively, for APP/PS1 and wild type mice at baseline and at 3h and 24h after a single administration of α-Ly6G or isotype control antibodies, and after 4 weeks of treatment every three days. APP/PS1 mice showed a modest trend toward taking more time to cross the 6-mm diameter beam as compared to wild-type controls. (c and d). Number of slips on the BBW for a 6- and 12-mm diameter beam, respectively, for APP/PS1 and wild type mice at baseline and at 3h and 24h after a single administration of α-Ly6G or isotype control antibodies, and after 4 weeks of treatment every three days. For both beam diameters, APP/PS1 mice showed significantly more slips while crossing the beam as compared to wild-type animals, suggesting a motor deficit in the APP/PS1 mice. All animal groups showed a reduction in the number of slips with subsequent trials, suggesting improved motor coordination with practice. This improvement did not appear different between α-Ly6G and isotype control treated APP/PS1 mice, suggesting that increases in brain blood flow did not influence the motor learning underlying the reduction in the number of slips. (e) Immobility time in forced swim test measured over 6 minutes for APP/PS1 and wild-type mice at baseline and at 3h and 24h after a single administration of α-Ly6G or isotype control antibodies, and after 4 weeks of treatment every three days (APP/PS1 Iso-Ctr: n=10 mice (5 female, 5 female), APP/PS1 α-Ly6G: n=10 mice (5 female, 5 male), wild-type α-Ly6G: n=11 mice (7 female, 4 male), wild-type Iso-Ctr: n=11 mice (8 female, 3 male). Boxplots are defined as: whiskers extend 1.5 times the difference between the value of the 75th and 25th percentile, median=black line and mean= red line. All data in this figure represents the aggregation of two independently-conducted sets of behavioral experiments.

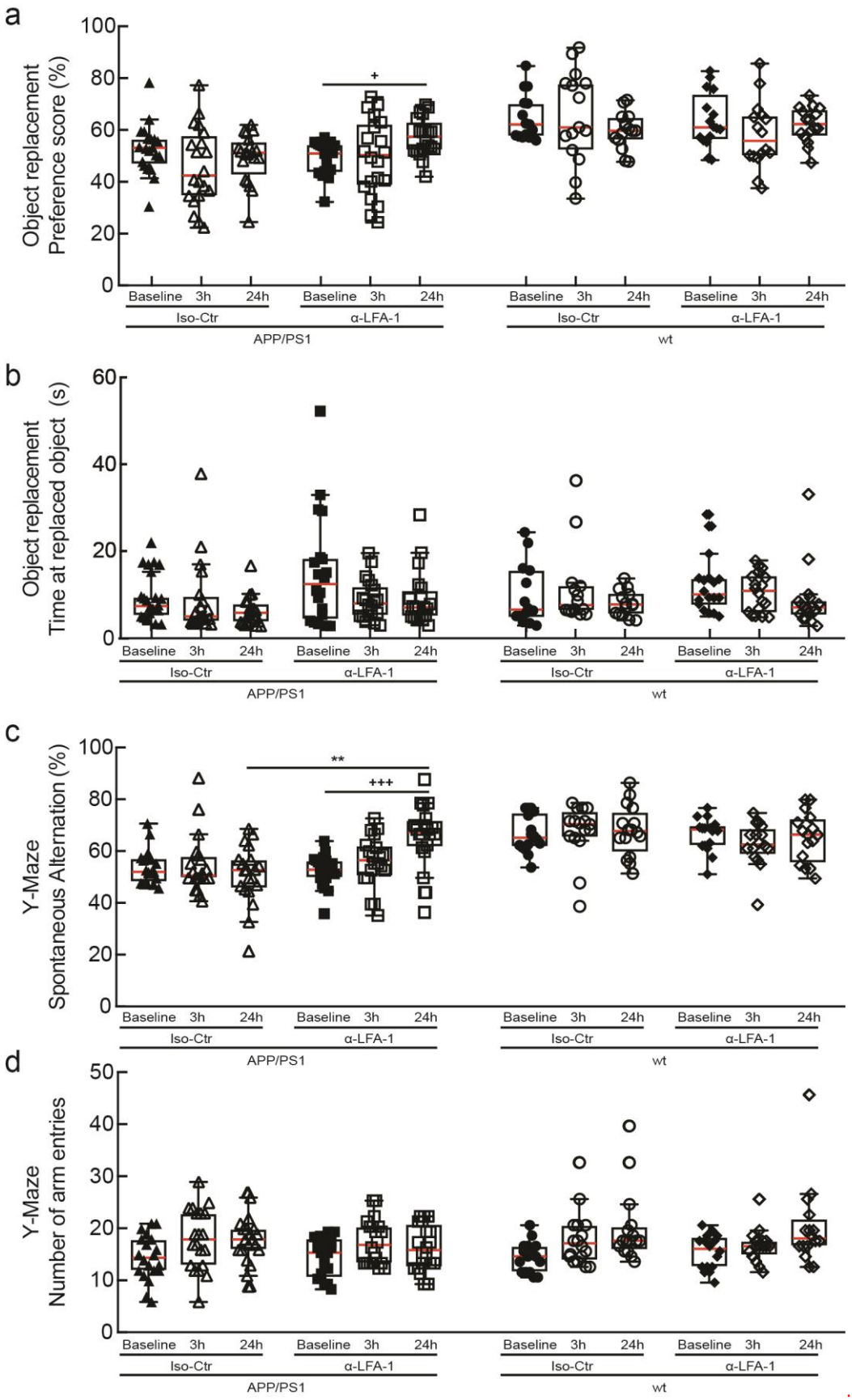
a
Object replacement
Preference score (%)
100
80
60
40
20
0
+
Baseline 3h 24h Baseline 3h 24h Baseline 3h 24h Baseline 3h 24h
Iso-Ctr
α-LFA-1
Iso-Ctr
α-LFA-1
APP/PS1
wt
b
Object replacement
Time at replaced object (s)
60
40
20
0
Baseline 3h 24h Baseline 3h 24h Baseline 3h 24h Baseline 3h 24h
Iso-Ctr
α-LFA-1
Iso-Ctr
α-LFA-1
APP/PS1
wt
c
Y-Maze
Spontaneous Alternation (%)
100
80
60
40
20
0
**
+++
Baseline 3h 24h Baseline 3h 24h Baseline 3h 24h Baseline 3h 24h
Iso-Ctr
α-LFA-1
Iso-Ctr
α-LFA-1
APP/PS1
wt
d
Y-Maze
Number of arm entries
50
40
30
20
10
0
Baseline 3h 24h Baseline 3h 24h Baseline 3h 24h Baseline 3h 24h
Iso-Ctr
α-LFA-1
Iso-Ctr
α-LFA-1
APP/PS1
wt

Supplementary Figure 13

Administration of α-LFA-1 improves performance of APP/PS1 mice on object replacement and Y-maze tests of spatial and working memory.

(a) Preference score in OR task at baseline and at 3 hr and 24 hr after a single administration of α-LFA-1 or Iso-Ctr antibodies in 11-13 month old APP/PS1 and wild-type mice. (b) Time spent at the replaced object measured over 3 minutes these mice at baseline and at 3h and 24h after a single administration of α-LFA-1 or isotype control antibodies. (c) Spontaneous alternation in Y-Maze task at baseline and at 3 hr and 24 hr after a single administration of α-LFA-1or Iso-Ctr antibodies. (d) Number of arm entries in the Y-maze measured for 6 minutes for APP/PS1 and wild-type mice at baseline and at 3h and 24h after a single administration of α-LFA-1 or isotype control antibodies. (APP/PS1 α-LFA-1: n=10 mice (6 female, 4 male); APP/PS1 Iso-Ctr: n=10 mice (6 female, 4 male); wild-type α-LFA-1: n=8 mice (5 female, 3 male); wild-type Iso-Ctr: n=7 mice (3 female, 4 male); one-way Kruskal-Wallis ANOVA with post-hoc pair-wise comparisons using Dunn's multiple comparison test: Y-maze APP/PS1 24hr (panel c) Iso-Ctr vs. α-LFA-1 p=0.0052; Friedman one-way repeated measures non-parametric ANOVA to compare baseline and after treatment results within a group: Object replacement APP/PS1 α-LFA-1 (panel a) baseline vs. 24hr p=0.035; Y-maze APP/PS1 α-LFA-1 (panel a) baseline vs. 24hr p=0.00040). Boxplots are defined as: whiskers extend 1.5 times the difference between the value of the 75th and 25th percentile, median=black line and mean= red line.

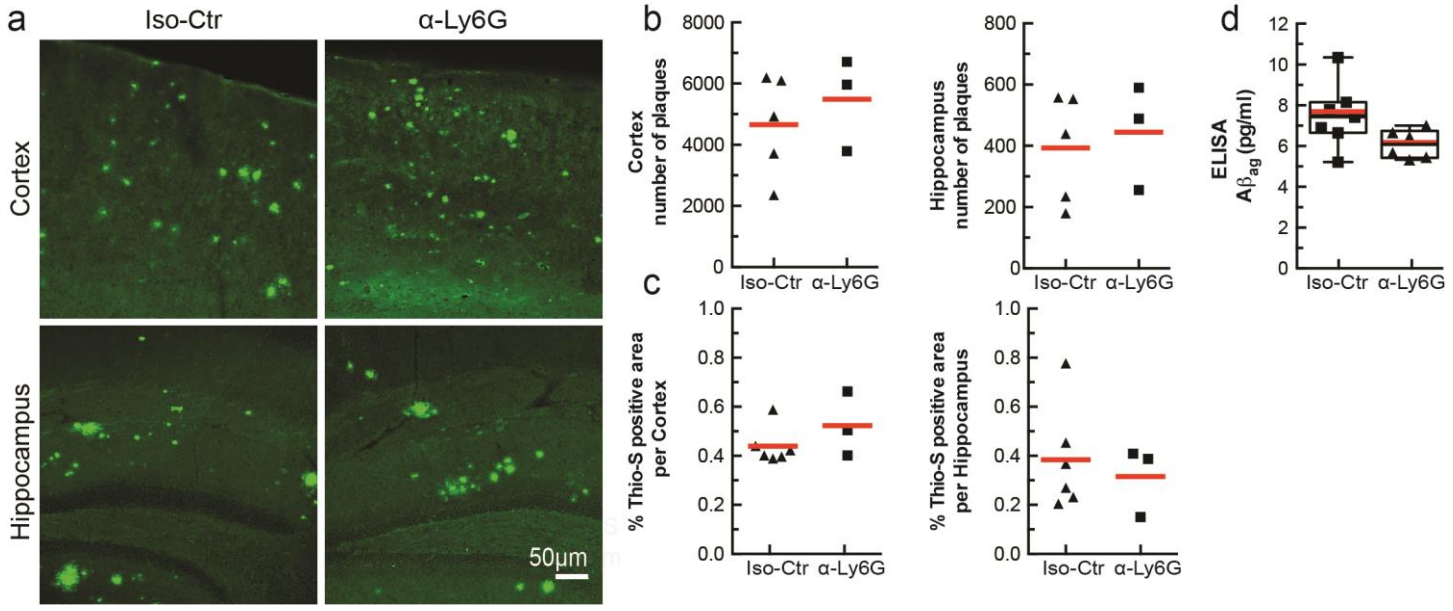

Supplementary Figure 14

Amyloid plaque density and concentration of amyloid-beta oligomers were not changed in 11-month-old APP/PS1 animals treated with α-Ly6G every 3 days for 1 month.

(a) Thioflavin-S staining of amyloid plaques in representative cortical sections (upper 2 panels) and hippocampal sections (lower 2 panels) for APP/PS1 mice treated with isotype control antibodies (left panels) or α-Ly6G (right panels). (b) Number of amyloid plaques in the cortex (left) and hippocampus (right) for APP/PS1 mice after one month of treatment (Iso-Ctr: n=5 mice (3 female, 2 male); α-Ly6G: n=3 mice (1 female, 2 male)). (c) Percentage of tissue section positive for Thioflavin-S in the cortex (left) and hippocampus (right) (Iso-Ctr: n=6 (3 female, 3 male); α-Ly6G: n=3 (1 female, 2 male)). Red line in b and c represents the mean. (d) ELISA measurements of Aβ aggregate concentrations after 4 weeks of treatment with α-Ly6G or isotype control antibodies every three days (Iso-Ctr: n=6 mice (4 female, 2 male) and α-Ly6G: n=7 mice (4 female, 3 male). Boxplots are defined as: whiskers extend 1.5 times the difference between the value of the 75th and 25th percentile, median=black line and mean= red line.

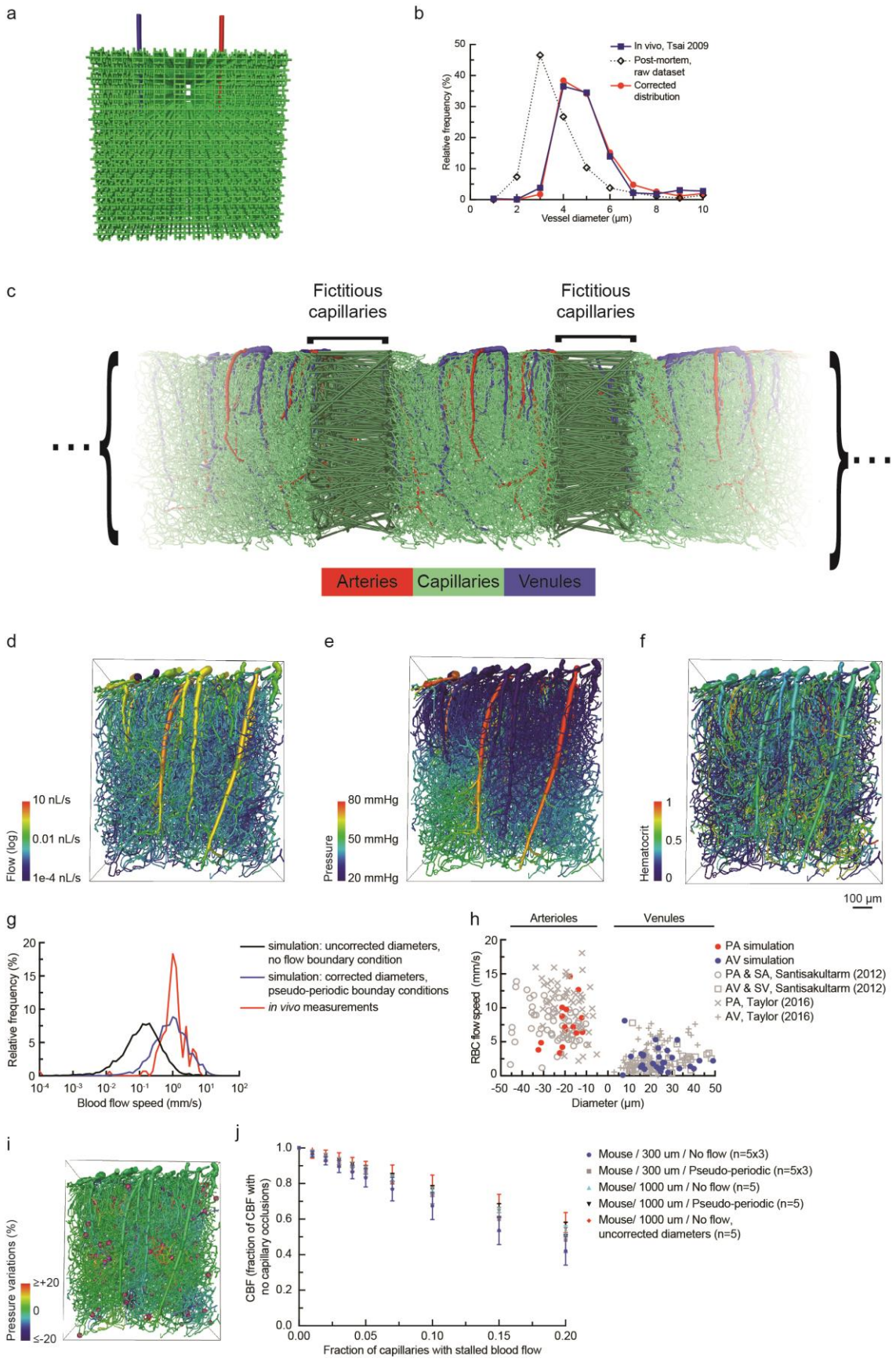
a
b
In vivo, Tsai 2009
Post-mortem, raw dataset
Corrected distribution
Relative frequency (%)
Vessel diameter (µm)
c
Fictitious capillaries
Fictitious capillaries
Arteries
Capillaries
Venules
d
Flow (log)
10 nL/s
0.01 nL/s
1e-4 nL/s
e
Pressure
80 mmHg
50 mmHg
20 mmHg
f
Hematocrit
1
0.5
0
100 µm
g
Relative frequency (%)
Blood flow speed (mm/s)
simulation: uncorrected diameters, no flow boundary condition
simulation: corrected diameters, pseudo-periodic bounday conditions
in vivo measurements
h
Arterioles
Venules
RBC flow speed (mm/s)
Diameter (µm)
PA simulation
AV simulation
PA & SA, Santisakultarm (2012)
AV & SV, Santisakultarm (2012)
PA, Taylor (2016)
AV, Taylor (2016)
i
Pressure variations (%)
≥+20
0
≤-20
j
CBF (fraction of CBF with no capillary occlusions)
Fraction of capillaries with stalled blood flow
Mouse / 300 um / No flow (n=5x3)
Mouse / 300 um / Pseudo-periodic (n=5x3)
Mouse/ 1000 um / No flow (n=5)
Mouse/ 1000 um / Pseudo-periodic (n=5)
Mouse/ 1000 um / No flow, uncorrected diameters (n=5)

Supplementary Figure 15

Periodization and vessel diameter scaling enabled matching of simulated distributions of arteriole, capillary, and venule flow speeds with published, experimentally measured values.

(a) Synthetic capillary network of order three. Capillaries are indicated in green, while red and blue indicate the single feeding arteriole and draining venule, respectively. (b) Histogram of mean mouse capillary diameters from *in vivo* measurements and post-mortem vascular casts. The diameter correction described in Eq. 5 closely aligned the post mortem diameters to the *in vivo* data. (c) Illustration of the pseudo-periodic boundary conditions. Vessels categorized as arterioles are labeled in red, venules in blue, and capillaries in green. Spatial distribution of simulated blood flow (d), pressure (e), and hematocrit (f) in each vessel in the mouse vascular network. (g) Comparison of red blood cell velocities in capillaries in the top 300-µm of mouse cortex from experimental, *in vivo* measurements (red line), simulations with pseudo-periodic boundary conditions with corrected diameters (blue line), and no-flow boundary conditions without corrected diameters (black line). (h) Relationship between red blood cell speed and vessel diameter in arterioles and venules in calculations (solid red and blue dots) and experimental measurements (grey points). (i) Pressure changes in mouse cortical vessel network due to randomly placed occlusions in 2% of capillaries. The corresponding flow changes are shown in Fig. 6a. (j) Calculated flow changes due to the occlusion of varying proportions of the capillaries using the full mouse dataset (1000 µm) or truncated datasets (1000x300 µm) with periodic or no flow boundary conditions, and with or without corrected vessel diameters (data points represent the mean and error bars represent the SD across five independent simulations; whole domain: n=5 simulations; 300 µm slices: n=5 simulations for each of 3 slices). Calculated blood flow decreases due to capillary stalls was robust with respect to simulation parameters.

Supplementary note on numerical simulations of cerebral blood flow changes induced by capillary occlusions for: "Neutrophil adhesion in brain capillaries reduces cortical blood flow and impairs memory function in Alzheimer's disease mouse models," by J.C. Hernandez, et al.

In previous work, we studied how the occlusion of a single cortical capillary influenced blood flow in downstream vessels[20] and found strong reductions in blood flow (10% of baseline value 1 branch downstream; 25% at 2 branches; 50% at 3 and 4 branches), suggesting that even the small fraction of occluded capillaries we observed in APP/PS1 mice could cause a significant decrease in overall brain blood flow. To test this idea, we simulated blood flow in anatomically accurate blood vessel networks from mice and humans and examined how flow changed when we occluded a random selection of capillaries.

Validation of simulations by comparison to in vivo measurements in mouse: As described in the Supplementary Methods, our simulations resulted in calculated values for flow (Supplementary Fig. 15d), pressure (Supplementary Fig. 15e), and hematocrit (Supplementary Fig. 15f) in each vessel segment in the volume. We validated the simulation by comparing *in vivo* measurements of blood flow at different levels in the microvascular hierarchy acquired by 2PEF from the top 300 μm of mouse cortex (data from Santisakultarm, *et al.*[53]) with the simulation predictions. The simulation results are highly dependent on the boundary conditions imposed on capillaries at the lateral edges of the simulation volume. The calculated velocity distribution using pseudo-periodic boundary conditions in capillaries up to 300 μm in depth and using the vessel diameter corrections described in the Supplementary Methods matches the experimental distribution well (Supplementary Fig. 15g). For comparison, the velocity distribution calculated using diameters from the raw datasets (without correction for the difference in vessel size between *in vivo* and post mortem measurements) and that calculated using a no-flow boundary condition both led to an order of magnitude underestimation of capillary flow speeds (Supplementary Fig. 15g). Our new pseudo-periodic boundary condition, together with the correction of vessel diameters, led to a velocity distribution that approaches the distribution of experimental velocities. The experimental distribution has a sharper peak, which might be due to experimental bias associated with

the limited number of vessels in which these measurements have been performed (147 *in vivo* measurements vs. 3,400 capillaries in the simulations). The simulated speeds in penetrating arterioles and ascending venules as a function of their diameters also closely matched experimental results from Santisakultarm, et al.[53] and from Taylor, et al.[61] (Supplementary Fig. 15h).

Numerical simulation of cerebral blood flow reductions caused by capillary occlusions: The effect of occlusions in capillaries was investigated by randomly selecting a given proportion of capillaries and reducing their flow by imposing a 100-fold reduction in diameter (pressure change: Supplementary Fig. 15i, flow change: Fig. 6a). To quantify the effects of the occlusions, we calculated the normalized cortical perfusion as the summed flow in the penetrating arterioles feeding the region, normalized by the value calculated with no capillary occlusions (Fig. 6c). While the magnitude of this summed flow is highly dependent on the boundary conditions, the decrease in flow due to capillary occlusions was much less sensitive to the choice of boundary conditions (Supplementary Fig. 15j). For the mouse network shown in Fig. 6a with pseudo-periodic boundary conditions and diameter correction, we found a linear decrease in the normalized perfusion with a slope S=-2.3±0.2 %baseline perfusion/% capillaries stalled (mean±SD) (Fig. 6c). This linear behavior was very robust to variations in the parameters chosen for the computations, with slopes equal to -2.2±0.1 (-2.1±0.2) with no-flow boundary conditions and diameter correction (no diameter correction). In order to evaluate the influence of boundary conditions with regard to the size of the simulated volume, 300 µm-thick sub-volumes of the mouse anatomical datasets were randomly extracted. The decrease in blood flow with increasing numbers of stalled capillaries was slightly larger when 300 µm-thick sub-volumes of the datasets were used (-2.6±0.4 and -2.9±0.5 with the pseudo-periodic boundary condition and the no-flow boundary condition, respectively), as compared to the full ~1 mm-thick volume. In Fig. 6c, only computations on the maximum simulation volume with the corrected diameters and pseudo-periodic boundary conditions are presented.

The simulations in the human network (Fig. 6b) using pseudo-periodic boundary conditions yielded a slope of S=-2.3±0.6, very similar to the mouse results. This linear decrease was also observed in synthetic periodic networks of order three (i.e. three edges per node; S=-2.9, Fig. 6c).

Limitations and methodological considerations: The human dataset used in the simulations was only 300 μm thick, raising concerns about the influence of boundary conditions. The broad agreement between simulation results in mouse datasets with 1-mm and 300-μm thickness reduces this concern. The simulations predicted a similar CBF increase across mouse and human vascular networks when stalls were reduced, suggesting that the blood flow improvements we observed in APP/PS1 mice may be achievable in humans.

The simulations predicted a smaller impact of capillary stalling on CBF than we observed experimentally. One possible explanation is that the simulations used vascular networks from wt mice, while AD mouse models have different vascular densities and topologies[71] that may influence the sensitivity of CBF to capillary stalls, although the vascular density differences between APP/PS1 and wt mice have been reported to be relatively minor[31,32]. In addition, increased leukocyte adhesion in APP/PS1 mice may lead not only to complete stalls, but also to slowed flow in some capillaries when a leukocyte is present in the segment, which is not captured in the simulations.

Supplementary Note-only References:

71 Brown, W. R. & Thore, C. R. Review: cerebral microvascular pathology in ageing and neurodegeneration. *Neuropathol Appl Neurobiol* **37**, 56-74, doi:10.1111/j.1365-2990.2010.01139.x (2011).

Supplementary Methods for: "Neutrophil adhesion in brain capillaries reduces cortical blood flow and impairs memory function in Alzheimer's disease mouse models," by J.C. Hernandez, et al.

Variations in surgical preparation and *in vivo* two-photon microscopy for TgCRND8 mice

Cranial window implantations were also performed in TgCRND8 mice (41-51 weeks of age, all female)[17]. These animals were housed at The Rockefeller University's Comparative Biosciences Center and treated in accordance with IACUC-approved protocols. The window implantation followed the same protocol as used for other animals, except that mice were anaesthetized using avertin (50 mg/100 g, intraperitoneal) and were given atropine (0.004 mg/100 g). For TgCRND8 mice, imaging was performed using a Fluoview 1000MPE two-photon laser scanning microscope (Olympus) equipped with a SpectraPhysics MaiTai DeepSee laser and a 25x/1.05 NA objective at The Rockefeller University Bio-Imaging Resource Center.

Awake imaging

A subset of mice was imaged with 2PEF without anesthesia. During the craniotomy surgery, a 3D-printed skull-attached mounting frame was secured on top of the cranial window to allow for head fixation during anesthesia-free imaging. The 3D-printed frame was flanked by 4 screws (TX000-1-1/2 self tapping screws, Small Parts Inc., Miami Lakes, FL) inserted into the skull. The screws and appropriate parts of the frame were glued to the skull using Loctite and dental cement to firmly attach the mounting frame.

We adapted and modified the awake imaging system from Dombeck et al.[52], in which a large (8 inch diameter) Styrofoam ball (Floracraft) was levitated using a thin cushion of air between the ball and a custom made (3D printed) casting containing eight 0.25 inch diameter air jets, arranged symmetrically. The air pressure was adjusted to just float the ball when the mouse was on top of it.

We trained mice to remain in a calm state during awake, head-fixed imaging. During the first training session, mice were handled, with the room lights on, by a trainer wearing gloves for ~10 min or until the mice routinely ran from hand to hand. The mice were then transferred to the ball and allowed to move freely for ~10 min with the room lights on while the handler rotated the ball to keep the mice centered near the top. The second training session consisted of again allowing the mice to move freely on the ball for ~10–15 min, again with the room lights on. The third training session began by head restraining the mice on the ball in complete darkness for ~15–20 min. Typically it would take 5–10 min for the mouse to learn to balance and then begin to walk or run. Mice were then head-fixed and placed on the ball during imaging under the microscope. Awake imaging lasted less than 30 min. Following awake imaging, mice were anesthetized as described above and imaging was repeated over the same cortical area to compare capillary physiology between the awake and anesthetized states.

Variations in quantification of capillary network topology and capillary segment stalling for 5xFAD mice

For the data on the fraction of capillaries stalled in the 5xFAD mice, individual capillary segments for categorization as flowing or stalled were identified using a more automated approach. Briefly, the image stack was preprocessed to the remove motion artifacts and noise. Then the vasculature network in the image stack was segmented using deep convolutional neural network followed by a post-processing procedure to extract the vectorized vasculature network[32]. Finally, each identified capillary segment was manually classified as either flowing or stalled.

Measurement of volumetric blood flow in penetrating arterioles

To quantify blood flow in cortical penetrating arterioles, we measured the vessel diameter from image stacks and the centerline RBC flow speed from line-scan measurements, as described in Santisakultarm *T.P.* et al.[53]. The volumetric blood flow, *F*, was calculated as:

$$F = \frac{\pi v r^2}{2} \qquad \text{Eq. 1,}$$

where v is the time-averaged centerline RBC speed and r is the vessel radius. To correlate the impact of the number of capillaries stalled on penetrating arteriole blood flow, we imaged the same capillaries and measured blood flow in the same six to eight penetrating arterioles in young APP/PS1 and wt mice (age 3-4 months), older APP/PS1 mice (age 11-14 months), and in 5xFAD and wt mice (age 5-7 months) treated with antibodies against Ly6G or with isotype control antibodies. Images to determine capillary stalling and line scans to determine penetrating arteriole blood flow speed were taken at baseline and at 60-90 min after treatment. All analysis was conducted blinded to the animal genotype, age, treatment, and imaging time point.

Amyloid plaque segmentation and density analysis

2PEF images of methoxy-X04 labeled amyloid plaques were filtered and binarized. Briefly, we first linearly interpolated the image stacks to have an isotropic 1 μm voxel size and then reduced the background signal in a line-by-line fashion by subtracting the median of each line. Salt and pepper image noise was reduced using the adaptive Wiener method with a 3 x 3 pixel kernel[54]. The image was then binarized using a manually-determined threshold (99% of the intensity distribution) and smoothed with a 3 x 3 pixel median filter. Objects smaller than 25 voxels were then removed, with object connectivity here defined as voxels sharing a face. The volume fraction of amyloid either globally or in a tube that follows the centerline of each capillary segment was then calculated from this binarized image. The tube volume was generated by swaying a sphere with a specified radius along the centerline of the capillary segment from one end to the other.

Kinetics of capillary stalling

To determine the short-term fate of capillaries that stalled, we repeatedly imaged the same capillary bed at baseline and at 5, 10, and 15 min later in APP/PS1 mice (n= 6 animals), and tracked the fate of all the capillaries that were stalled at baseline. If a vessel was observed as

stalled at all subsequent imaging time points, it was scored as remaining stalled, and if flow had resumed the stall was scored to have resolved. If the originally stalled capillary resumed flow, then re-stalled at a later time point that was scored as re-stalled. In some animals, we further determined the cause of capillary stalls at each of these time points.

To evaluate the longer-term fate of capillaries that were stalled, we imaged APP/PS1 mice (n= 5 animals) at baseline and then 1, 3, 7, and 14 days later and determined what fraction of the capillaries stalled at baseline were stalled at any subsequent imaging session.

We estimated how frequently we would observe capillaries stalled at baseline to be stalled at any subsequent imaging session assuming that no stalls lasted long enough to stay stalled between imaging sessions and that each capillary segment was equally likely to stall. With this model, the probability, P_c, of the capillaries stalled at baseline to be stalled at any subsequent imaging session is:

$$P_c = 1 - (1 - r)^N \qquad \text{Eq. 2,}$$

where r is the fraction of capillaries with stalled blood flow and N is the number of observations after the baseline imaging.

Flow cytometry of circulating neutrophil counts

To determine the impact of α-Ly6G on neutrophil number, we used flow cytometry to determine neutrophil counts 3, 6 and 24 hr after a single treatment (4 mg/kg) and after one month of treatment every three days (2 mg/kg).

Blood from APP/PS1 and wt mice was collected from the submandibular vein and mixed with 1x RBC lysis buffer (00-4300-54, ThermoFisher Scientific). After incubation at room temperature for 10 min, the sample was centrifuged at 500 g for 5 min and the supernatant was removed. The cell pellet was re-suspended in 500 uL of Hank's balanced salt solution (HBSS) supplemented with 1% bovine serum albumin (BSA) and centrifuged again; this washing procedure was repeated 3 times. Following isolation, neutrophils were re-suspended at a density of 10^7 cells per ml in HBSS supplemented with 1% BSA. The cell samples were labeled at room temperature for 45 min with the following anti-mouse

antibodies: anti-CD45 (560695, BD Bioscience), anti-CD11b (557686, BD Bioscience) and anti-Ly6G (551460, BD Bioscience). After washing the samples with HBSS samples have been re-suspended in FACS buffer (1% BSA and 2mM EDTA in PBS), the remaining leukocytes were analyzed by flow cytometry using a Guava easyCyte Flow Cytometer (EMD Millipore Corporation). Data were analyzed using FlowJo software (FlowJo LLC). The neutrophil population was identified based on the side and forward scatter and later gated for $CD45^{high}$, $CD11b^{high}$, and $Ly6G^{high}$ using FlowJo.

Measurement of global blood flow using ASL-MRI

Imaging was performed on a 7.0 Tesla small animal MRI system with 450 mT/m gradient amplitude and a 4500 T/m/s slew rate (Biospec 70/30, Bruker). The animals were anesthetized with isoflurane in oxygen and immobilized in the MRI using a nose cone and bite ring. A volume coil was used for transmission and a surface coil for reception. We imaged APP/PS1 and wt mice (age 7-9 months) at baseline. About 48 hrs later, animals were given an intraperiotenial injection of α-Ly6G or isotype control antibodies (4 mg/kg) and a second set of images were acquired between 2-6 hr after injection. Mice were randomly assigned to receive treatment or isotype control antibodies and the experimenter was blinded to both mouse genotype and whether the antibody was the treatment or control during the experiment.

Anatomical images were acquired to find a coronal slice at a location approximately 1 mm caudal to Bregma[55]. This position was used for subsequent ASL imaging, which was based on a FAIR-RARE pulse sequence that labeled the inflowing blood by global inversion of the equilibrium magnetization[56]. In this method, inversion recovery data from the imaging slice are acquired after selective inversion of the slice and after inversion of both the slice and the surrounding tissue. The difference of the apparent R1 relaxation rate images then yields a measure of the CBF[57]. Three averages of one axial slice were acquired with a field of view of 15 × 15 mm, spatial resolution of 0.23 × 0.23 × 2 mm^3, echo time TE of 5.36 ms, effective TE of 26.84 ms, repeat time TR of 10 s, and a RARE factor of 36. This resulted in a total scan time for the CBF images of about 25 min. Turbo-RARE anatomical images were acquired with the following parameters: 10 averages of 14 slices with the same field-of-view and orientation

as the ASL images, resolution = 0.078 × 0.078 × 1 mm^3, TE = 48 ms, TR = 2000 ms, and a RARE factor of 10. The total scan time was about 6 min.

For computation of CBF, the Bruker ASL perfusion processing macro was used. It uses the model and includes steps to mask out the background and ventricles described in Kober, et al.[58]. The masked CBF images were exported to Analyze format on the MRI console. We then used the anatomical image to create a mask that outlined the entire cortical region, excluding the sinus, and averaged the CBF measurement across this region for each animal at each imaging time point. Analysis of ASL-MRI data was conducted by a researcher blinded to animal genotype, imaging time point, and treatment.

Multi-Exposure Laser Speckle Imaging

Mice were anesthetized for imaging using 3% isoflurane for induction and were given atropine and glucose each hour as described above. Depth of anesthesia was monitored using a force-sensitive square resistor placed below the mouse to detect respiration. For imaging, anesthesia was reduced to 1.5% in medical air and then adjusted to maintain a respiration rate between 65-75 breaths per minute. The mouse temperature was maintained at 37°C with a feedback-controlled heating pad.

Multi-exposure laser speckle contrast imaging quantifies the degree of blurring of a laser speckle pattern due to moving scatterers for different image exposure times[59]. In the cortex, moving red blood cells are the primary moving scatterers, so this technique yields a measure of cerebral blood flow. Images were taken using a near-IR camera (Basler) through a 4x objective (NA=0.28, Olympus) with a 786-nm stabilized laser diode (LD785-SEV300, ThorLabs), intensity modulated using an acousto-optic modulator (AOMO 3100-125 and AODR 1110AF-AEFO-1.5, Gooch & Housego). Laser speckle images were taken at 15 exposure times ranging across three decades from 50 μs to 80 ms, as described by Kaszmi et al.[60], with a calibrated laser intensity for each exposure time. Images were taken at ~10 fps with 30 images for each exposure time at each time point.

Mice were imaged for 20 minutes prior to antibody injection in order to ensure stabilization under anesthesia. Animals received either α-Ly6G or isotype control antibodies (4mg/kg,

intraperitoneal). The mice were imaged for 3 hours post-injection.

Speckle contrast values, *K*, were fitted to the equation:

$$K^2(T,\tau_c) = \beta\rho^2 \frac{e^{-2x}-1+2x}{2x^2} + 4\beta\rho(1-\rho)\frac{e^{-x}-1+x}{x^2} + v_e \qquad \text{Eq. 3}$$

with $x = \frac{T}{\tau_c}$

where τ_c is the correlation time, considered to be inversely proportional to average speed of moving scatterers in the sample, T is the exposure time, ρ is the fraction of dynamically scattered light, v_e accounts for any noise in the system, and β is a normalization constant indicating the mismatch between speckle and pixel sizes. The β parameter is estimated using the simpler form of the equation where ρ is considered to be 1:

$$K^2(T,\tau_c) = \beta \frac{e^{-2\frac{T}{\tau_c}}-1+2\frac{T}{\tau_c}}{2(\frac{T}{\tau_c})^2} + v_e \qquad \text{Eq. 4}$$

Fractional blood flow changes are proportional to the inverse of the correlation time image divided by a baseline image taken immediately before antibody injection.

Additional behavior experiments

Forced swim test: The forced swim test measured depression-like behavior. Mice were individually placed in a 4-L glass beaker filled with 2.5 L of 25°C water. Mice were allowed to adjust for 1 min and then were evaluated for 6 min. An experimenter blind to the genotype and treatment analyzed the videotaped behavior and scored the immobility time, defined by the absence of active, escape-oriented behaviors such as swimming, jumping, rearing, sniffing, or diving.

Balance beam walk: The balance beam walk measured motor coordination and balance by scoring the ability of the mice to traverse a graded series of narrow beams to reach an enclosed safety platform. The beams consisted of long strips of wood (80 cm) with a round cross section of 12- or 6-mm diameter. The beams were placed horizontally, 40 cm above the floor, with one end mounted on a narrow support and the other end attached to an enclosed platform. Bright light illuminated the end of the beam where the mice started. Mice received

three consecutive trials on each of the round beams, in each case progressing from the widest to the narrowest beam (15 min between each trial). Mice were allowed up to 60 s to traverse each beam. The time to traverse each beam and the number of times either hind paw slipped off each beam were recorded for each trial. Analysis of each measure was based on the mean score across all trials for that mouse at that time point. Experimenters were blinded to the genotype and the treatment of the mice.

Extraction of network topology and vessel diameters from mouse anatomical dataset

One large postmortem dataset from the vibrissa primary sensory (vS1) cortex in mouse previously obtained by Tsai et al[21] and Blinder et al.[44], was used for this study (~1 mm^3 and ~15,000 vessel segments). In brief, this dataset was obtained by filling the vessels with a fluorescent indicator, extracting the brain and imaging with 2PEF from the pial surface to near the bottom of cortex. In this dataset, penetrating arterioles and ascending venules that reached the pial surface were identified by following their connections to a large cerebral arteriole or venule. We further labeled subsurface vessels in three classes: arterioles, capillaries, and venules. Starting with the surface and penetrating arterioles (venules) vessels were classified by iteratively seeking all vessels with diameter above 6 μm connected to any previously labeled arteriole (venule). All remaining vessels were labeled as capillaries. The diameter threshold was manually chosen as the smallest integer diameter value which resulted in arteriolar and venular trees that exhibited no loops, in contrast to the very looped capillary network.

Due to post-mortem shrinkage, vessel diameters in this mouse dataset were smaller than those measured *in-vivo*, so required rescaling[21,44,53]. As blood flow is highly dependent on vessel diameters, two successive corrections were applied. First, a monotonically increasing function, which tends to one at large diameters, was applied to all vessels diameters:

$$d = d_0 + A\cos\left(\tan^{-1}\left(\frac{d_0}{B}\right)\right), \quad A > 0, \quad B > \frac{2}{3}A\sin\left(\tan^{-1}\left(\frac{1}{\sqrt{2}}\right)\right) \qquad \text{Eq. 5}$$

where d is the corrected diameter and d_0 is the diameter extracted from the image stack. A and B are constrained parameters calculated so that the corrected vessel diameter

distribution matched *in vivo* measurements from two photon microscopy[21], as shown in Supplementary Fig. 15b. This function ensures that the hierarchy of diameters in the network is preserved and the larger vessels are not rescaled. For the network represented in Fig. 6a, A=1.4 and B=10.3, so that the diameter threshold for capillary vessels becomes 7.2 μm. A second depth-dependent correction was then applied to the diameter of arterioles and venules:

$$d = d_0(az + b) \quad \text{Eq. 6}$$

where z is the depth below the cortical surface and a and b are parameters determined so that the diameters of the trunks of the penetrating arterioles and ascending venules matched *in-vivo* measurements[61]. For the network represented in Fig. 6a, these parameters were a=-0.0014 μm^{-1} (-9.36e-4 μm^{-1}) and b=2.54 (2.02) for arterioles (venules).

Extraction of network topology and vessel diameters from human anatomical dataset

The dataset used was previously obtained by Cassot et al.[62] and Lauwers et al.[22] from thick sections (300 μm) of a human brain injected with India ink from the Duvernoy collection[63]. The brain came from a 60-year old female who died from an abdominal lymphoma with no known vascular or cerebral disease. It corresponds to a large volume (6.4 mm^3 of cerebral cortex) extending across 20.8 mm^2 along the lateral part of the collateral sulcus (fisiform gyrus) extracted from Section S2 in Lauwers et al.[22], and includes a total of 27,340 vessel segments. The mean radius and length of each segment were rescaled by a factor of 1.1 to account for the shrinkage of the anatomical preparation. The main vascular trunks were identified manually and divided into arterioles and venules according to their morphological features, following Duvernoy's classification[63,64]. Following Lauwers et al.[22] and Lorthois et al[23] as in the mouse data sets, arterioles (venules) were defined by iteratively seeking all vessels with diameter above 9.9 μm connected to any previously identified arteriole (venule), so that no loops were present. All remaining vessels were classified as capillaries.

Synthetic network generation

The synthetic periodic network of order three (i.e. three edges per node) was generated to match the mouse network parameters. A 1-mm^3 vascular network was constructed by replication of a simple periodic network (Supplementary Fig. 15c). Capillary diameters and lengths were uniform and were set to the averages for the mouse network. A single penetrating arteriole and ascending venule (with diameters set to the averages from the mouse network) served as inlet/outlet. The distance between the inlet and outlet corresponded to the average distance between penetrating arterioles and ascending venules from the mouse dataset.

Blood flow simulations

The methodology for simulating blood flow in these intra-cortical vascular networks has been presented in detail in Lorthois et al.[23]. Briefly, the network was represented by a graph in which edges represent vessel segments between branches that are characterized by an average diameter and length. We used a one-dimensional (analogous to electric circuit models) nonlinear network model that was slightly modified from Pries et al.[65] to handle large networks for the flow simulations. Using an iterative procedure, the model takes into account the complex rheological properties of blood flow in the microcirculation (Fåhræus, Fåhræus-Lindqvist, and phase separation effects). These effects are modeled using empirical descriptions[66,67] deduced from experiments in rats. The model was used to calculate the flow and hematocrit in each vessel and the pressure at each intersection of vessels. For the human dataset, the parameters for the empirical descriptions of the Fåhræus, Fåhræus -Lindqvist and phase separation effects were re-scaled in order to account for the difference in characteristic size between human and rat RBCs, as proposed by Lorthois et al.[23] and Roman et al.[68]. This simulation approach has no free parameters.

Boundary conditions: Physiologically realistic pressure drops of 60 mmHg, as measured in rats[69] and estimated in humans[23], were imposed between all arteriolar and venular trunks feeding and draining the computational volume, while a no-flow condition was imposed on deeper arteriolar or venular vessels that intersected the lateral boundaries of the simulated

volume. A constant discharge hematocrit of 0.45, corresponding to a typical value of the systemic hematocrit, was also imposed in arteriolar trunks. Moreover, a pseudo-periodic boundary condition was applied to all capillaries at the lateral boundaries, as illustrated in Supplementary Fig. 15c. Fictitious vessels were created that link capillaries intersecting opposing faces in a semi random fashion. A grid was created on the two faces and refined until, for a given cell, each capillary on one face was matched with at most 2 capillaries on the opposing face, allowing the creation of fictitious bifurcations. Once the optimal grid was found, the closest neighboring vessels from the opposing faces were connected together. The length of the resulting fictitious vessels was set to 50 μm and their diameters to the average diameters of the connected capillaries. This pseudo-periodic boundary condition is similar in spirit but simpler and more computationally effective than the one recently introduced by Schmid et al.[70]. Finally, a no-flow boundary condition was applied to all vessels intersecting the bottom face of the domain. We also compared the results with no-flow boundary conditions for all capillaries at the lateral boundaries.

Simulating stalls: In order to study the influence of capillary stalling on cerebral blood flow, a given proportion of capillaries in each network was randomly occluded. To simulate occlusion, the radius of the selected vessels was divided by 100. This resulted in a large increase of the hemodynamic resistance, of order 10^8, and a similar decrease of the computed flow through these vessels. At least five repetitions were performed for each proportion of stalled capillaries and each set of conditions considered. On the mouse data, about 1000 simulations in total were run on a 32-core Intel(R) Xeon E5-2680 v2 @ 3.3 GHz for a total computational time of ~170 hours. For human data set, about 100 simulations were run on the same machine for a total computational time of ~50 hours.

Histopathology

Immunohistochemistry was performed on the brains of mice chronically treated every third day for 4 weeks with either α-Ly6G antibody or isotype control (Iso-Ctr n=5, α-Ly6G n=4). A single paraformaldehyde-fixed hemisphere of each brain was cut into 40 μm thick sagittal sections.

Every sixth section from each mouse was stained with 1% Thioflavin-S (T1892**,** Sigma) for 10 min at room temperature and washed twice with 80% ethanol for 2 min. The sections were mounted using Fluoroshield with DAPI (F6057, Sigma). Images were taken using confocal microscopy (Zeiss Examiner.D1 AXIO). For each image, the background was subtracted using the ImageJ background subtraction plugin (Rolling ball with 7 μm radius). Images were then manually thresholded, using the same threshold for all sections from a given mouse. Appropriate thresholds varied mouse to mouse and were set to ensure that the smallest Thioflavin-S labeled objects that morphologically appeared to be an amyloid plaque remained above threshold. Cortical and hippocampal regions of interest were defined in each section anatomically, and the fraction of pixels above threshold was determined across all sections for these regions of interest. All image processing was done blinded to treatment group. As a second measure of amyloid deposition, we manually counting the number of Thioflavin-S positive amyloid plaques in the cortex and hippocampus, again across all sections and while blinded to the treatment group. All sections were stained and imaged in parallel. Artifacts such as bubbles were eliminated from analysis by manually excluding these regions.

Sample size determinations

In most cases, sample sizes for comparisons across groups were determined from power analysis calculations. The data on capillary stall incidence in Fig. 1c and d in APP/PS1 vs. wt mice is significantly overpowered, as this data includes experiments that yielded the initial discovery of elevated capillary stalling in APP/PS1 mice as well as all subsequent baseline data. For measurements of the cellular cause of capillary stalls (Fig. 2a and b), we anticipated finding ~20 stalls per mouse (~2% of 1,000 characterized capillaries). Assuming each possible stall cause was equally likely and wanting to resolve these percentages to ±10% at a 95% confidence interval, then binomial statistics implied the need for ~100 capillary stalls, or about five mice. For 2PEF measurements of penetrating arteriole blood flow (Fig. 3b and c), ASL-MRI measurements of cortical perfusion (Fig. 3d and e), and behavioral experiments (Fig. 4) comparing APP/PS1 and wt mice before and after antibody treatment, we used a matched-pairs study design, estimates of measurement variability from published and

preliminary data, and estimates of minimal biologically-relevant effect size to determine minimum group sizes using G*Power. This yielded minimum group sizes of 5 mice for 2PEF measurements of penetrating arteriole blood flow and 10 mice for ASL-MRI and behavioral experiments. In subsequent experiments with other mouse models and other treatments we continued using these group sizes.

Supplementary Methods-only References:

52 Dombeck, D. A., Khabbaz, A. N., Collman, F., Adelman, T. L. & Tank, D. W. Imaging large-scale neural activity with cellular resolution in awake, mobile mice. *Neuron* **56**, 43-57, doi:10.1016/j.neuron.2007.08.003 (2007).

53 Santisakultarm, T. P. *et al.* In vivo two-photon excited fluorescence microscopy reveals cardiac- and respiration-dependent pulsatile blood flow in cortical blood vessels in mice. *American journal of physiology. Heart and circulatory physiology* **302**, H1367-1377, doi:10.1152/ajpheart.00417.2011 (2012).

54 Lim, J. *Two-Dimensional Signal and Image Processing*. (Prentice Hall, 1990).

55 Paxinos, G. & Franklin, K. *The mouse brain in stereotaxic coordinate*. (Elsevier Academic Press, 2004).

56 Kim, S. G. Quantification of relative cerebral blood flow change by flow-sensitive alternating inversion recovery (FAIR) technique: application to functional mapping. *Magn Reson Med* **34**, 293-301 (1995).

57 Herscovitch, P. & Raichle, M. E. What is the correct value for the brain--blood partition coefficient for water? *J Cereb Blood Flow Metab* **5**, 65-69, doi:10.1038/jcbfm.1985.9 (1985).

58 Kober, F. *et al.* High-resolution myocardial perfusion mapping in small animals in vivo by spin-labeling gradient-echo imaging. *Magn Reson Med* **51**, 62-67, doi:10.1002/mrm.10676 (2004).

59 Dunn, A. K. Laser speckle contrast imaging of cerebral blood flow. *Ann Biomed Eng* **40**, 367-377, doi:10.1007/s10439-011-0469-0 (2012).

60 Kazmi, S. M., Parthasarthy, A. B., Song, N. E., Jones, T. A. & Dunn, A. K. Chronic imaging of cortical blood flow using Multi-Exposure Speckle Imaging. *J Cereb Blood Flow Metab* **33**, 798-808, doi:10.1038/jcbfm.2013.57 (2013).

61 Taylor, Z. J. *et al.* Microvascular basis for growth of small infarcts following occlusion of single penetrating arterioles in mouse cortex. *J Cereb Blood Flow Metab* **36**, 1357-1373, doi:10.1177/0271678X15608388 (2016).

62 Cassot, F., Lauwers, F., Fouard, C., Prohaska, S. & Lauwers-Cances, V. A novel three-dimensional computer-assisted method for a quantitative study of microvascular networks of the human cerebral cortex. *Microcirculation* **13**, 1-18, doi:10.1080/10739680500383407 (2006).

63 Duvernoy, H. M., Delon, S. & Vannson, J. L. Cortical blood vessels of the human brain. *Brain Res Bull* **7**, 519-579 (1981).

64 Reina-De La Torre, F., Rodriguez-Baeza, A. & Sahuquillo-Barris, J. Morphological characteristics and distribution pattern of the arterial vessels in human cerebral cortex: a scanning electron microscope study. *Anat Rec* **251**, 87-96 (1998).
65 Pries, A. R., Secomb, T. W., Gaehtgens, P. & Gross, J. F. Blood flow in microvascular networks. Experiments and simulation. *Circ Res* **67**, 826-834 (1990).
66 Pries, A. R., Secomb, T. W. & Gaehtgens, P. Biophysical aspects of blood flow in the microvasculature. *Cardiovasc Res* **32**, 654-667 (1996).
67 Pries, A. R., Reglin, B. & Secomb, T. W. Structural response of microcirculatory networks to changes in demand: information transfer by shear stress. *American journal of physiology. Heart and circulatory physiology* **284**, H2204-2212, doi:10.1152/ajpheart.00757.2002 (2003).
68 Roman, S., Merlo, A., Duru, P., Risso, F. & Lorthois, S. Going beyond 20 mum-sized channels for studying red blood cell phase separation in microfluidic bifurcations. *Biomicrofluidics* **10**, 034103, doi:10.1063/1.4948955 (2016).
69 Bragin, D. E., Bush, R. C., Muller, W. S. & Nemoto, E. M. High intracranial pressure effects on cerebral cortical microvascular flow in rats. *J Neurotrauma* **28**, 775-785, doi:10.1089/neu.2010.1692 (2011).
70 Schmid, F., Tsai, P. S., Kleinfeld, D., Jenny, P. & Weber, B. Depth-dependent flow and pressure characteristics in cortical microvascular networks. *PLoS Comput Biol* **13**, e1005392, doi:10.1371/journal.pcbi.1005392 (2017).